SMITH COLLEGE

Smith ScholarWorks

Geosciences: Faculty Publications

Geosciences

11-1-2019

Holocene and Last Interglacial climate of the Faroe Islands from sedimentary plant wax hydrogen and carbon isotopes

Lorelei Curtin
Lamont-Doherty Earth Observatory

William J. D'Andrea
Lamont-Doherty Earth Observatory

Nicholas Balascio
William & Mary

Genevieve Pugsley
William & Mary

Gregory de Wet
University of Massachusetts Amherst, gdewet@smith.edu

See next page for additional authors

Follow this and additional works at: https://scholarworks.smith.edu/geo_facpubs

 Part of the Geology Commons

Recommended Citation

Curtin, Lorelei; D'Andrea, William J.; Balascio, Nicholas; Pugsley, Genevieve; de Wet, Gregory; and Bradley, Raymond, "Holocene and Last Interglacial climate of the Faroe Islands from sedimentary plant wax hydrogen and carbon isotopes" (2019). Geosciences: Faculty Publications, Smith College, Northampton, MA.
https://scholarworks.smith.edu/geo_facpubs/146

This Article has been accepted for inclusion in Geosciences: Faculty Publications by an authorized administrator of Smith ScholarWorks. For more information, please contact scholarworks@smith.edu

Authors

Lorelei Curtin, William J. D'Andrea, Nicholas Balascio, Genevieve Pugsley, Gregory de Wet, and Raymond Bradley

This article is available at Smith ScholarWorks: https://scholarworks.smith.edu/geo_facpubs/146

Version of Record: https://www.sciencedirect.com/science/article/pii/S0277379119304251
Manuscript_f34c5e14f3565ec4f4bbb3c2b1405646

Holocene and Last Interglacial climate of the Faroe Islands from sedimentary plant wax hydrogen and carbon isotopes

Authors: Lorelei Curtin[a,b*], William J. D'Andrea[a], Nicholas Balascio[c], Genevieve Pugsley[c], Gregory de Wet[d], Raymond Bradley[d]

Affiliations:

[a] Lamont-Doherty Earth Observatory, Columbia University, 61 Route 9W, Palisades, NY

[b] Department of Earth and Environmental Sciences, Columbia University, New York, NY

[c] Department of Geology, The College of William & Mary, Williamsburg, VA

[d] Department of Geosciences, University of Massachusetts, Amherst, MA

[*]corresponding author: lcurtin@ldeo.columbia.edu. Lamont-Doherty Earth Observatory, 104 Geoscience, 61 Route 9W, Palisades, NY 10964.

Abstract:

The Last Interglacial period (LIG) is Earth's most recent globally warm period and is analogous in some ways to projected future global warming. However, questions remain regarding the state of the climate during the LIG in the North Atlantic, a region that is extremely sensitive to changes in oceanic and atmospheric circulation. Here, we present hydrogen and carbon isotope (δD and $\delta^{13}C$) records from a suite of plant wax biomarkers preserved in Holocene and LIG lacustrine sediments from the North Atlantic Faroe Islands and interpret them as qualitative proxies for temperature and hydroclimate variability. These data are used to directly compare LIG and Holocene climate using the same proxy approaches from the same terrestrial location.

© 2019 published by Elsevier. This manuscript is made available under the Elsevier user license
https://www.elsevier.com/open-access/userlicense/1.0/

Measuring multiple isotopes on multiple types of waxes elucidates the sources of homologous plant waxes. We deduce that the δD values of long-chain *n*-alkanes (C_{27}-C_{33}) and mid-chain *n*-alkanes (C_{23}-C_{25}) in these sedimentary archives reflect leaf water and lake water δD values, respectively, while the δD values for both long-chain (C_{28}-C_{30}) and mid-chain n-alkanoic acids (C_{24}-C_{26}) primarily represent lake water δD values. Plant wax-inferred δD values of precipitation during the early Holocene (10,100 to 8,200 cal yr BP) are ~35‰ more positive than late Holocene values, and decline over the Holocene. δD-inferred hydrologic change and $\delta^{13}C$ -inferred plant water use efficiency both indicate that the Faroe Islands became drier throughout the Holocene. Comparison with measurements from LIG plant waxes indicates that late LIG in the Faroe Islands was hydrologically similar to the early- to mid-Holocene (8,200 to 4,000 cal yr BP), with enriched precipitation isotopes and reduced evapotranspiration indicating a warmer, wetter environment.

Keywords: Paleoclimatology; Holocene; Interglacial; North Atlantic; Organic Geochemistry; Stable Isotopes

1. Introduction

To better understand how Earth's climate system will respond to anthropogenic warming, it is important to document climate patterns during warm periods of Earth's history. The Last Interglacial period (LIG; ~130 ka to 116 ka) was warmer than the preindustrial period in most regions (CAPE-Last Interglacial Project Members, 2006; Kukla et al., 2002; McKay et al., 2011; Otto-Bliesner et al., 2013; Turney and Jones, 2010), and is analogous in some ways to future warming scenarios. Climate reconstructions for the LIG have been developed using a variety of climate proxies from terrestrial and marine archives (Figure 1) (Axford et al., 2009; Bauch et al., 1999; Björck et al., 2000; Cortijo et al., 1994; De Beaulieu and Reille, 1992; Kühl and Litt, 2003; Mangerud et al., 1981; Mcfarlin et al., 2018; Salonen et al., 2018; Shackleton et al., 2003; Zagwijn, 1996 and others). However, the magnitude of warming relative to modern temperature and the hydrological conditions of the terrestrial North Atlantic region during the Holocene and LIG have not been well documented.

Amplification of warming at high latitudes makes understanding the climatic conditions of the North Atlantic and Arctic during past warm periods particularly important (Holland and Bitz, 2003; Manabe and Stouffer, 1980; Serreze and Francis, 2006). Furthermore, deep water convection in the northern North Atlantic and Nordic Seas region is a critical component of the Atlantic Meridional Overturning Circulation and oceanographic changes in the North Atlantic have been linked to abrupt climate changes globally (e.g. Younger Dryas, 8.2 ky event, Bond events, Dansgaard-Oeschger cycles) (Behl and Kennett, 1996; Broecker et al., 1990; Clark et al., 2002; Peterson et al., 2000; Wang et al., 2001). Most of our current understanding of LIG

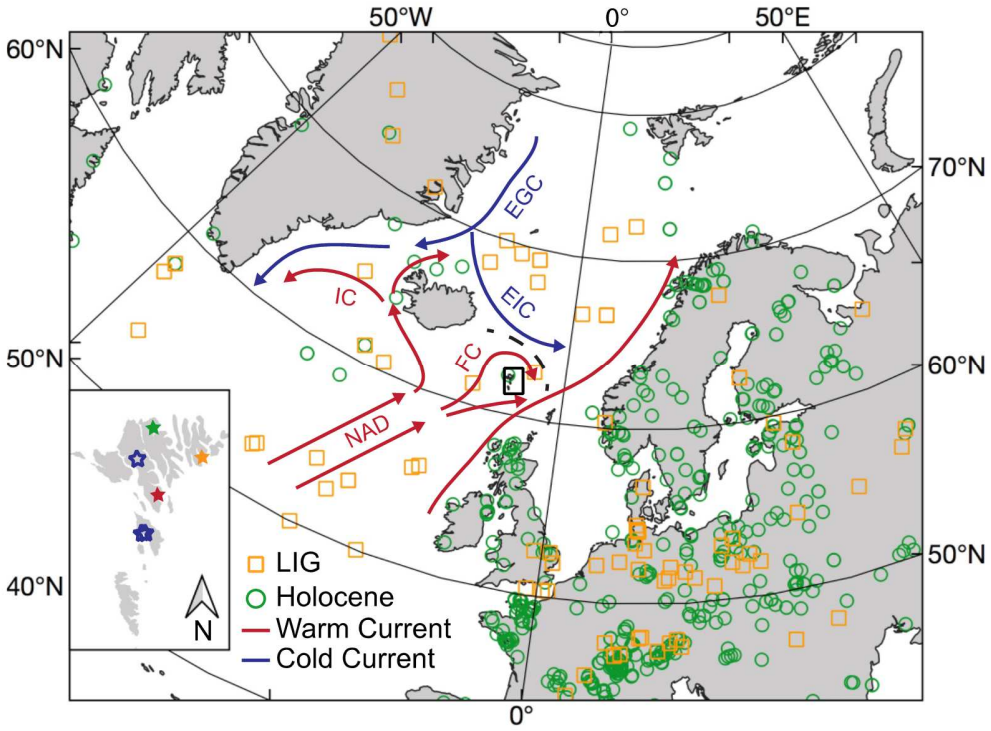

Figure 1. Map of the North Atlantic region, marked with published full-Holocene (green circle) and LIG (yellow square) quantitative paleotemperature records (locations from Kaspar et al., 2005; Turney and Jones, 2010; Marcott et al., 2013; Sundqvist et al., 2014; Marsicek et al., 2018). Inset is the Faroe Islands, with a green star marking lake Eiðisvatn, yellow star marking the Klaksvík LIG section, red star marking the location of the instrumental climatological record, and blue stars marking the three locations where modern lake water isotope samples were taken. Red arrows and labels show warm surface ocean currents (NAD: North Atlantic Drift, FC: Faroes Current, IC: Irminger Current), while blue arrows and labels show cold surface currents (EGC: East Greenland Current, EIC: East Iceland Current). Black dashed line marks the Faroe-Iceland Front

conditions in the North Atlantic region comes from marine sediment records, which do not document terrestrial climate. While terrestrial paleorecords from Europe suggest that LIG temperatures were 2-3°C warmer than modern (Kaspar et al., 2005), records of sea surface temperatures are inconsistent regarding the difference in temperature between the LIG and Holocene. Some marine records show LIG temperatures up to 10°C warmer than modern or preindustrial temperatures (Bauch et al., 1999; CLIMAP Project Members, 1984; Oppo et al., 2006), others suggest mean annual temperatures were as much as 2.6°C cooler during the LIG (Bauch et al., 1999; CLIMAP Project Members, 1984), and still others indicate no difference at all (Cortijo et al., 1994). It is still unclear if the large differences in LIG temperature reconstructions are due to uncertainties in the climate proxies or actual regional differences in LIG temperatures. Modeling studies of LIG temperatures also yield conflicting results for the North Atlantic, with some showing up to 4-6°C of warming relative to modern (McKay et al., 2011; Otto-Bliesner et al., 2013; Pfeiffer and Lohmann, 2016) while others suggest cooler temperatures or little to no difference (Gierz et al., 2017).

While most previous studies of the LIG have focused on marine records, terrestrial records of precipitation isotopes have the potential to reveal new information regarding atmospheric conditions during the LIG. Hydrogen and oxygen isotope values (δD and $\delta^{18}O$) of precipitation vary spatially across Earth's surface and reflect atmospheric circulation patterns and other aspects of Earth's climate and hydrological cycle. In the North Atlantic, precipitation isotopes are anomalously enriched in deuterium (D) and ^{18}O for their latitude, due to the northeastward transport of heat and moisture into the region by oceanic and atmospheric circulation (Bowen and Revenaugh, 2003). Therefore, times of reduced ocean heat transport and atmospheric heat

and moisture transport to the northern North Atlantic from southwesterly sources are characterized more negative isotopic values of precipitation. For example, a modeling study of the 8.2 ky cooling event suggests that the isotopes in precipitation across in this region would have become more negative during cold periods with reduced meridional overturning circulation (LeGrande and Schmidt, 2008). It follows that during past warm intervals, such as the LIG and the early Holocene, the isotopic composition of precipitation would have been more positive; however, this has not been well documented across the North Atlantic region.

The Faroe Islands are located between Iceland and Scotland, where the climate is strongly influenced by the magnitude of ocean and atmospheric heat and moisture transport into the northern North Atlantic and the Nordic Seas. Because precipitation isotopes in the North Atlantic region are not only sensitive to local changes in temperature, but more broadly reflect regional ocean and atmospheric circulation patterns, records of past precipitation isotopes from terrestrial sediment archives on the Faroe Islands document past changes in regional climate and oceanographic conditions. While lakes containing Holocene-length sedimentary records are ubiquitous in the North Atlantic region, terrestrial LIG sedimentary archives are rare because the region was extensively glaciated during the last glacial period. On the Faroe Islands a LIG-aged lacustrine sedimentary unit survived the last glaciation and provides an archive of LIG climate information (Bennike et al., 2018; Geikie, 1881; Wastegård et al., 2005). Thus, LIG climate conditions in the Faroes can be directly compared to Holocene climate by reconstructing precipitation isotopes from both Holocene and LIG lake sediments.

Past precipitation isotopes can be reconstructed using the δD value of hydrogen contained in plant wax molecules, which are well preserved in lake sediments. The hydrogen isotope composition of plant waxes reflects the isotopic composition of the plant's source water, after modification due to biosynthetic fractionation and evaporative enrichment (Kahmen et al., 2013; Sachse et al., 2012, 2004; Sauer et al., 2001). Plant waxes are deposited and preserved in lake sediment and can therefore be used to reconstruct the isotopic composition of their source water through time (Sachse et al., 2012). The hydrogen isotope fractionation between source water and plant wax can vary between plant types, species, and individuals (Chikaraishi et al., 2004; Chikaraishi and Naraoka, 2007; Diefendorf et al., 2011; Zhang and Sachs, 2007), and therefore large shifts in vegetation within the watershed can affect a sedimentary plant wax hydrogen isotope record (Feakins, 2013). Despite such potentially confounding factors, the strong relationship between δD values of plant waxes and δD values of precipitation has been demonstrated in studies from across the world (Hou et al., 2008; Polissar and Freeman, 2010; Sachse et al., 2012, 2004 and references therein).

Here, we present Holocene and LIG records of plant wax hydrogen and carbon isotopes ($\delta^{13}C$) from the Faroe Islands, which we use to infer past changes in precipitation isotopes and hydroclimate. The objectives of this study are to document the Holocene evolution of climate in the Faroe Islands, and to compare the Holocene to late-LIG climate using the same paleoclimate proxies. The Holocene record we present is derived from lake sediments from Eiðisvatn and the LIG record from an exposure of lacustrine sediment near Klaksvík on Borðoy (Figure 1). We report results from multiple plant wax types (*n*-alkanes and *n*-alkanoic acids), chain lengths, and isotope systems (δD and $\delta^{13}C$) to evaluate the sources of plant waxes and the environmental

103 signals reflected by the sedimentary plant wax δD from these locations. We use $\delta^{13}C$
104 measurements to constrain the provenance of the leaf waxes and as an independent means of
105 understanding changes in hydrologic conditions through changes in water use efficiency of
106 plants. Faroe Island precipitation isotopes during the late LIG were very similar to those of the
107 early to mid-Holocene, and all of these were enriched in deuterium relative to preindustrial
108 values. We conclude that regional ocean and atmospheric conditions in the late LIG were similar
109 to those in the early to mid-Holocene.
110
111 **2. Study Area**
112
113 *2.1 Background*
114 The Faroe Islands are an archipelago of 18 islands located between Iceland and Scotland and
115 between the Norwegian Sea and the North Atlantic (62°N, 7°W; Figure 1). The islands are the
116 remnants of a Tertiary flood basalt platform that erupted during the opening of the North Atlantic
117 Basin (Rasmussen and Noe-Nygaard, 1970). The climate of the Faroes is strongly connected to
118 local oceanographic conditions. The archipelago is located in the main pathway of the warm
119 northward flowing North Atlantic Drift, and the cold East Iceland current approaches the Faroes
120 from the northwest (Figure 1). The boundary between cold and warm currents, the Iceland-Faroe
121 Front, is located to the north of the Faroe Islands. Winters are mild and summers are cool (Figure
122 2), and the precipitation is largely sourced from storms that approach from the southwest
123 (Cappelen, 2018). Annual precipitation amounts vary from 1000 mm/yr at lower elevations to
124 3000 mm/yr at high elevations in the northwest (Cappelen, 2018).

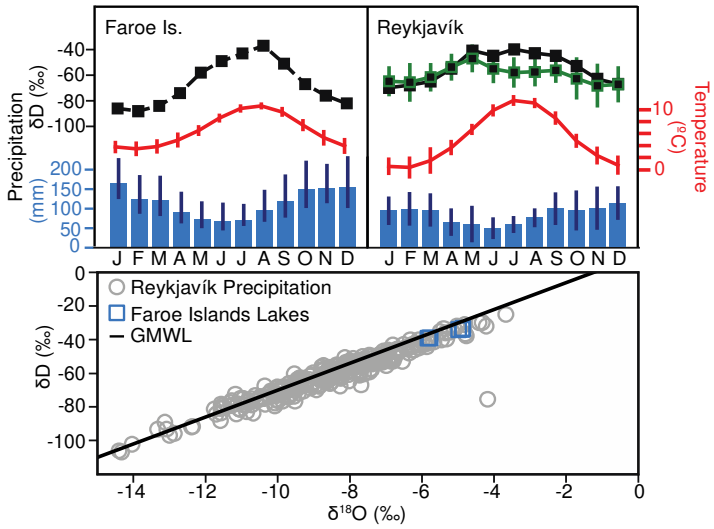

125 Figure 2. Top panels: Faroe Islands and Reykjavík climatology and precipitation isotopes.
126 Reykjavík climatology and precipitation isotopes are from the Global Network of Isotopes in
127 Precipitation database, which includes monthly average amount-weighted precipitation isotopes
128 (green squares with one standard deviation error bars), temperatures (red line with one standard
129 deviation error bars), and precipitation amounts (blue bars with one standard deviation error
130 bars) from 1960 to 2018. Faroe Islands climatology is from published technical reports from the
131 Danish Meterological Institute (Cappelen, 2018), which includes monthly average temperature
132 (red line with one standard deviation error bars) and precipitation amounts (blue bars with one
133 standard deviation error bars) from 1992-2018 in Tórshavn. Black squares indicate OIPC
134 modeled precipitation isotopes. Bottom panel: grey circles indicate δD and $\delta^{18}O$ values of all
135 precipitation samples from Reykjavik from GNIP. Blue squares indicate δD and $\delta^{18}O$ values of
136 water samples from Faroese lakes collected in August of 2015. Black line indicates the GMWL.
137
138
139

140 The closest Global Network of Isotopes in Precipitation (GNIP) station to the Faroe Islands is in
141 Reykjavík, Iceland approximately 800 km away. Climate conditions in Reykjavík are similar to
142 those in the Faroes (Figure 2), and precipitation δD values at Reykjavik have a seasonal range of
143 ~20‰. The Online Isotopes in Precipitation Calculator suggests an even larger seasonal range of
144 ~50‰ in the Faroe Islands (Bowen, 2019) based on interpolation of existing precipitation isotope
145 data (Bowen et al., 2005). However, the OIPC overestimates the seasonal range in the isotopes of
146 precipitation for Reykjavík compared to the GNIP measurements (Figure 2), so it is possible that
147 the seasonal range modeled for the Faroe Islands is similarly overestimated. The North Atlantic
148 Oscillation (NAO) is the dominant mode of inter-annual atmospheric variability in the North
149 Atlantic region and is strongly correlated with precipitation isotopes in central Europe and in the
150 North Atlantic high latitudes, however, no correlation has been found between the NAO and the
151 isotopes of precipitation in the Faroe Islands (Baldini et al., 2008).
152
153 The Faroes were covered by a local ice cap during the last glacial period (Jørgensen and
154 Rasmussen, 1986). Basal dates from lake sediment cores indicate that deglaciation occurred
155 ~11,700—12,100 cal yr BP (Andresen et al., 2006; Olsen et al., 2010), probably coincident with
156 the end of the Younger Dryas cold period. The sediments that have accumulated in Faroese lakes
157 since the local deglaciation provide high-resolution archives of paleoenvironmental conditions
158 throughout the Holocene. A general understanding of Holocene environmental history in the
159 Faroes has been gained through various palynological and geochemical studies of lake sediments
160 across the archipelago (Hannon et al., 2010, 2003, 2001, 1998; Jessen et al., 2008; Johansen,
161 1985, 1981, 1975; Lawson et al., 2005, 2008, 2007; Olsen et al., 2010). Human settlement of the
162 Faroes occurred late in the Holocene (within the last ~2000 years), and so unlike most European

sites, the Holocene records are largely undisturbed by human activities. Most archaeological evidence points to settlement by the Norse in the 9th century A.D. (Arge et al., 2005; Hannon et al., 2001), although there is some palynological and archaeological evidence that suggests earlier settlement (Hannon et al., 2005, 2001; Hannon and Bradshaw, 2000; Johansen, 1985; Church et al., 2013).

2.2 Study Sites

Eiðisvatn is located on the northern end of the island of Eysturoy at 62°17'10.3"N, 7°03'27.4"W. The lake has a surface elevation of 129 m above sea level and had a surface area of 0.47 km^2 prior to construction of a hydroelectric dam in the late 1980s, which expanded the lake area. Several small inlets flow into the lake, and tunnels bring water from neighboring valleys into the lake today. Before the lake was dammed, there was one major outlet stream. Eiðisvatn, like other hydrologically open lakes on the Faroes, likely has lake water isotope values that are very similar to precipitation (Figure 2).

An organic-rich sediment deposit laying between two glacial till deposits is located at 62°13'25.2"N, 6°34'22.2"W in a coastal cliff section near Klaksvík, on Borðoy in the Faroe Islands (Geikie, 1881). The section is approximately 1m thick, and is composed of silt and clay (Bennike et al., 2018). Total organic content of the sediment decreases from ~6% near the bottom to 2% at the top (Wastegård et al., 2005). Radiocarbon analyses of pieces of wood found in the unit yielded infinite ages (Rasmussen, 1972), and the deposit has since been stratigraphically assigned as late LIG via the occurrence of the 5e-Midt/RHY tephra throughout

186 the section (Wastegård et al., 2005). Macrofossil, sedimentological and diatom analyses all
187 indicate that the sequence represents a lacustrine environment with occasional marine overwash
188 deposits (Bennike et al., 2018; Wastegård et al., 2005).
189
190 **3. Methods**
191
192 *3.1 Chronology and loss on ignition*
193
194 Two gravity cores, EI-D-01-15 (73.7 cm) and EI-D-02-15 (100.7 cm) were collected from the
195 lake to preserve the sediment-water interface. The top 10cm of EI-D-01-15 were extruded and
196 subsampled in the field. A 2.82m piston core, EI-P-01-15, was also collected using a percussion
197 coring device. 17 terrestrial plant macrofossils and 4 bulk sediment samples were collected from
198 the two surface cores and the piston core for AMS ^{14}C measurements. Samples were treated with
199 a base-acid-base sequence to remove carbonate and humic contamination, combusted, and
200 graphitized for measurement at either the UC-Irvine W. M. Keck Carbon Cycle AMS Laboratory
201 or at the Woods Hole NOSAMS Laboratory.
202
203 Sediment samples ($1cm^3$) from three visible tephra layers in the core were digested in 10% H_2O_2
204 to remove organic matter, washed over a 63 μm sieve using deionized water, and subjected to
205 heavy-liquid density separations to isolate material with densities of 2.3-2.5 g/cm^3 (Blockley et
206 al., 2005; Turney et al., 1997). Samples were then mounted on glass slides in epoxy resin,
207 examined using light microscopy, and polished to expose grain interiors. Major oxide
208 geochemical compositions were determined using wavelength-dispersive spectroscopy on an

209 ARL-SEMQ electron microprobe equipped with six wavelength-dispersive spectrometers and a
210 Bruker 5030 SDD energy-dispersive spectrometer at the Concord University Microanalytical
211 Laboratory (WV, USA) using a 6μm beam diameter, 14 kV accelerating voltage, and 10 nA
212 beam current. Reported data are non-normalized oxide concentrations with each datum
213 representing a single analysis of one tephra grain. Glass shard compositions were compared to
214 previously described tephra horizons from the Faroe Islands (as reviewed by Wastegård et al.,
215 2018).
216
217 Twenty-one radiocarbon and the three identified tephras were used to build an age model for the
218 Holocene sediment using the Bayesian framework calibration software code 'Bacon' in R
219 (Blaauw and Christen, 2011), using the IntCal13 calibration curve (Reimer et al., 2013). Eight
220 radiocarbon samples were found to have anomalously old ages and were excluded from the final
221 age model.
222
223 Weight loss-on-ignition (LOI) was measured on $1cm^3$ subsamples at 1cm intervals in EI-D-02-15
224 and EI-P-01-15 following Heiri et al. (2001). Gravity and piston cores were aligned on a
225 composite depth scale by aligning wt. % LOI measurements.
226
227 *3.2 Organic and stable isotope geochemistry*
228
229 1 cm-thick samples were taken from the piston core every 10cm, along with the top 1cm of each
230 of the gravity cores, for lipid biomarker analysis. Samples were freeze-dried and then
231 homogenized using a ceramic mortar and pestle. Lipids were extracted from the sediment

samples using a Dionex Accelerated Solvent Extractor with a 9:1 solution of dichloromethane (DCM) and methanol. Each sample was subjected to three five-minute extraction cycles at 100°C and 1000psi.

Compounds in the total lipid extract were separated using silica gel flash column chromatography over 0.75g of solvent-rinsed 100% activated silica gel. Aliphatic, ketone, and polar fractions were separated by successive elution with 4ml of hexane, DCM, and methanol, respectively. Solid-phase aminopropyl column chromatography was used to isolate n-alkanoic acids from the polar fraction, by successive elution with 4 mL of 2:1 DCM:isopropanol and 4% acetic acid in diethyl ether. The second fraction, which contained the n-alkanoic acids, was methylated overnight at 50°C using 2% HCl in methanol to form n-alkanoic acid methyl esters for analysis. The straight chain n-alkanoic acid methyl esters were separated from hydroxyl acid esters and other polyfunctional compounds using silica gel flash column chromatography with 4ml of hexane and DCM as eluents. The DCM fraction containing the *n*-alkanoic acid methyl esters, and the original hexane fraction from the first silica gel separation containing n-alkanes, were dried under N_2 gas and reconstituted in 100uL of hexane for analysis.

n-Alkanes and *n*-alkanoic acids were identified and quantified using an Agilent 7890A gas chromatograph equipped with a mass selective detector (MSD) and a flame ionization detector (FID) using a 30m-long DB-5 capillary column with an internal diameter of 250 um. Initial GC oven temperature was set to 60 °C, then ramped to 150°C at 15°C per minute, and then ramped to 320°C at 4°C per minute. Compounds were identified by comparison of the mass spectra and retention times to an *n*-alkane standard containing C_{10}-C_{40} *n*-alkanes (Sigma Aldrich Supelco 40147-u) and an *n*-alkanoic acid standard solution containing the even *n*-alkanoic acids from C_8-

C_{32} (Nu-Chek prep mixture 19A and Larodan mixture Me 277). The external standards were used to determine compound-specific FID peak area response factors and to quantify compounds of interest in each sample.

δD and $\delta^{13}C$ values of *n*-alkanes and n-alkanoic acids were measured via GC-IRMS on a Thermo Trace GC coupled to a Thermo Delta V through an Isolink Conflo IV. Sample D/H and $^{13}C/^{12}C$ measurements were referenced to the VSMOW and VPDB scales, respectively, according to the recommendations of Polissar and D'Andrea (2014) and using Mix A5 and Mix A7 standards with 15 *n*-alkane molecules whose D/H and $^{13}C/^{12}C$ were determined offline by Arndt Schimmelmann at the University of Indiana. All sample isotope ratios are reported using standard δ notation,

$$\delta D, \delta^{13}C = \left(\frac{R_{sample}}{R_{VSMOW,\ VPDB}} - 1\right) \times\ 1000. \quad (1)$$

where R = D/H or $^{13}C/^{12}C$. *n*-Alkanoic acid δD and $\delta^{13}C$ values were mathematically corrected for methyl group addition by analyzing the δD and $\delta^{13}C$ of a sample of phthalic acid that was methylated alongside sample *n*-alkanoic acids. Results were processed and pooled analytical uncertainties (1 s.e.m.) in sample δD and $\delta^{13}C$ values were calculated and reported according to Polissar and D'Andrea, 2014.

3.3 Biomarker indices

Average chain lengths (ACL) of *n*-alkanes and *n*-alkanoic acids were calculated using the formula

277 $$ACL_{alk,acid} = \frac{\sum(C_i)(X_i)}{\sum C_i} \quad (2)$$

278 where C_i is the concentration of a given *n*-alkane or *n*-alkanoic acid relative to total alkane or n-
279 alkanoic acid concentration, X_i is the carbon chain length, and i = odd numbers from 21 to 35 for
280 *n*-alkanes and even numbers from 20 to 34 for *n*-alkanoic acids (Poynter and Eglinton, 1990).
281
282 Deuterium fractionation between terrestrially-sourced *n*-alkanes (C_{29}, C_{31}, and C_{33}) and
283 aquatically-sourced *n*-alkanes (C_{25} and C_{27}) ($\varepsilon_{2Hterr\text{-}2Haq}$) was calculated using standard epsilon
284 notation:

285 $$\varepsilon_{2Hterr-2Haq} = 1000\left[\frac{(\delta D_{terr} + 1000)}{(\delta D_{aq} + 1000)} - 1\right]. \quad (3)$$

286 *n*-Alkanes were designated terrestrial vs. aquatic based on the trends in δD values and the carbon
287 isotope values (discussed in section 5.1). Carbon fractionation between *n*-alkanes and their
288 biosynthetically equivalent *n*-alkanoic acids ($\varepsilon_{13Calk\text{-}13Cacid}$) are also expressed in standard epsilon
289 notation, such that:

290 $$\varepsilon_{13Calk-13Cacid} = 1000\left[\frac{(\delta^{13}C_{n-alkane} + 1000)}{(\delta^{13}C_{n-alkanoic\ acid} + 1000)} - 1\right]. \quad (4)$$

291 Intrinsic water use efficiency (iWUE), defined as the amount of carbon assimilated per water
292 transpired, can be calculated according to the following equation (Ehleringer et al., 1993; Feng,
293 1999):

294 $$iWUE = \frac{c_a - c_i}{1.6}, \quad (5)$$

295 where c_a is the concentration of CO_2 outside a leaf and c_i is the concentration of CO_2 in the leaf
296 intercellular space. C_i values can be calculated according to the following equation:

297 $$1000\left[\frac{(\delta^{13}C_{atm}+1000)}{(\delta^{13}C_{plant}+1000)}-1\right]=a+(b-a)\frac{c_i}{c_a}, \quad (6)$$

298 where $\delta^{13}C_{atm}$ is the $\delta^{13}C$ value of atmospheric CO_2, $\delta^{13}C_{plant}$ is the $\delta^{13}C$ value of bulk plant
299 material, a is the fractionation associated with gas diffusion into the leaf (~-4.4‰), and b is the
300 fractionation associated with the Rubisco enzyme during carboxylation (~-27‰). The apparent
301 fractionation between bulk plant and *n*-alkanes is approximately 6‰ (Chikaraishi and Naraoka,
302 2001; Collister et al., 1994). Using pCO_2 and $\delta^{13}C_{atm}$ values from ice cores (Elsig et al., 2009;
303 Lourantou et al., 2010; Monnin et al., 2004), c_i and iWUE can be calculated from $\delta^{13}C$ values of
304 terrestrially sourced leaf waxes.
305
306 **4. Results**
307
308 *4.1 Holocene chronology*
309
310 The stratigraphy and geochemistry of tephra deposits on the Faroe Islands are well-characterized
311 (Wastegård et al., 2018). Major oxide compositions from the Eiðisvatn glass shards are
312 compared to previously identified tephra and cryptotephra horizons from the Faroe Islands and
313 we attribute volcanic glass shards isolated from three discrete depth intervals in the
314 Eiðisvatn record to the Hekla S, Hekla 4 and Saksunarvatn eruptions (Figure 3; Tables 1, S1,
315 S2). These three tephras, along with 13 radiocarbon dates, were used to build an age-depth model
316 for the Eiðisvatn sediment core (Table 2, Figure 4).
317
318
319

Table 1. Geochemical composition of glass shards isolated from the Eiðisvatn record compared to tephra identified at other Faroe Islands sites.

Sample		SiO_2	TiO_2	Al_2O_3	FeO	MnO	MgO	CaO	Na_2O	K_2O	P_2O_5	Cl	BaO	Total
Eidi 138.9 cm (n=15)	*Mean*	65.5	0.45	14.7	5.75	0.16	0.55	3.35	4.47	2	0.19	0.1	0.1	97.3
	1s	1.11	0.02	0.37	0.21	0.02	0.03	0.11	0.19	0.1	0.04	0	0	1.44
Hekla S (n=15)[1, 3]	*Mean*	66.6	0.4	14.7	5.28	0.16	0.48	3.21	4.45	2	0.11	-	-	97.3
	1s	2.32	0.11	0.46	1.09	0.04	0.16	0.8	0.55	0.4	0.04	-	-	1.49
Eidi 156.9 cm (n=19)	*Mean*	62.7	0.63	14.1	8.25	0.26	0.5	4.14	4.38	1.8	0.18	0.1	0.1	97
	1s	1.93	0.13	0.46	0.99	0.03	0.21	0.35	0.57	0.2	0.07	0	0	1.6
Hekla 4 (n=22)[1]	*Mean*	63.8	0.62	14.2	7.73	0.26	0.58	3.95	4.43	1.9	-	-	-	97.3
	1s	3.91	0.23	0.59	2.31	0.08	0.3	1.06	0.32	0.4	-	-	-	0.98
Eidi 301.5 cm (n=24)	*Mean*	48.7	3.05	12.9	14.6	0.22	5.02	9.95	2.61	0.5	0.32	0	0	97.9
	1s	0.61	0.49	0.2	0.31	0.02	0.33	0.19	0.2	0.1	0.1	0	0	0.7
Saksunarvatn (n=43)[1, 2]	*Mean*	48.9	3.03	12.9	14	0.25	5.58	9.83	2.74	0.5	0.33	-	-	97.8
	1s	0.71	0.14	0.26	0.5	0.03	0.18	0.32	0.19	0	0.02	-	-	1.2

References: 1. Wastegård et al. (2001), 2. Kylander et al. (2012), 3. Wastegård et al. (2018)

320

321

322 *4.1.1 EI-P-01-15 138.9 cm/Hekla S (c. 3.7 ka BP)*

323 The major oxide composition of dacitic to rhyolitic glass shards (n=15) isolated from the interval
324 116.5-117.5 cm closely resembles the 3.7 ka Hekla Selsund (Hekla S) tephra horizon, which was
325 previously identified in sediments from Faroese lakes Starvatn (Wastegård et al., 2008),
326 Mjáuvötn (Wastegård et al., 2001), and Havnardalsmyren (Wastegård et al., 2018). The
327 composition of Hekla S deposits on the Faroe Islands varies between sites, likely due to
328 geochemical differences between early and late eruption phases (Wastegård et al., 2018). Hekla
329 S glass shards isolated from the Eiðisvatn record are geochemically similar to rhyolitic shards
330 previously identified in sediments from Mjáuvötn and Havnardalsmyren (Wastegård et al., 2018,

2001), but distinct from andesitic shards found in sediments from Starvatn (Wastegård et al., 2008).

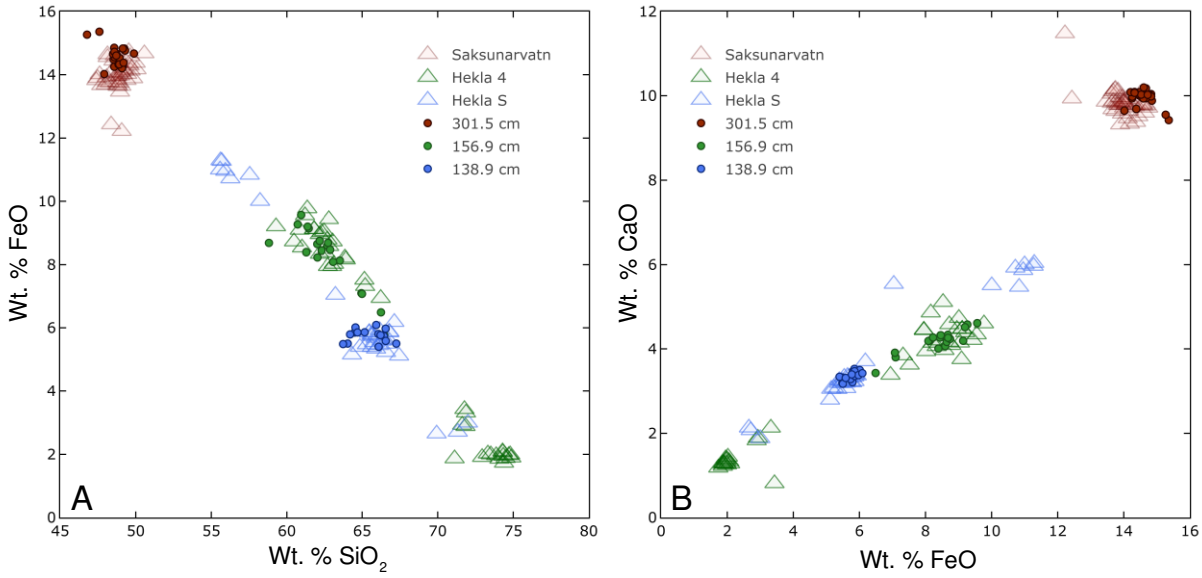

Figure 3. Select major oxide compositions of three tephra layers from the Eiðisvatn record compared to previously described Icelandic tephra deposits on the Faroe Islands: (A) SiO_2 vs. FeO, (B) FeO vs. CaO. Glass shards from Eiðisvatn are compared to Hekla S (Wastegård et al., 2001, 2008, 2018), Hekla 4 (Hannon et al., 2001; Wastegård et al., 2001, 2018), and Saksunarvatn (Wastegård et al., 2001; Kylander et al., 2012).

4.1.2 EI-P-01-15 156.9 cm/Hekla 4 (c. 4.3 ka BP)

We attribute dacitic to andesitic glass shards from the 135-136 cm depth interval (n=19) to the Hekla 4 eruption c. 4.3 ka BP. As with Hekla S, the geochemical composition of Hekla 4 shards identified from the Faroe Islands is spatially heterogeneous. Tephra shards attributed to Hekla 4 from the Eiðisvatn core are geochemically similar to Hekla 4 glass shards previously found in bog sediments on the southwestern margin of Eiðisvatn, in lake sediments from Mjáuvötn

346 (Wastegård et al., 2001) and a subset of shards from Havnardalsmyren (Wastegård et al., 2018;
347 Table 1; Figure 3). Their composition differs from rhyolitic shards found in sediments from
348 Gróthusvatn (Hannon et al., 2001) and Havnardalsmyren that were attributed to Hekla 4
349 (Wastegård et al., 2018).

Table 2. Chronological data used to construct Eiðisvatn age model.

Core	Composite	Description	^{14}C age (yr	Calibrated age	Median

350

	Depth (cm)		BP)	range (cal yr BP, 1σ)	age (cal yr BP)
Surface	0				-65
EI-D-01-15	18.5	Plant macrofossil	-10	-5 - -1	-3
EI-D-01-15	23	Plant macrofossil	410 ± 15	471-515	493
EI-P-01-15	25.86	Plant macrofossil	840 ± 30	710-784	747
EI-P-01-15	27.86	Plant macrofossil	3720 ± 70	3964-4176	4070*
EI-P-01-15	29.86	Plant macrofossil	2575 ± 20	2714-2760	2737*
EI-D-01-15	30	Plant macrofossil	1145 ± 15	986-1068	1027
EI-P-01-15	32.86	Plant macrofossil	2320 ± 20	2331-2355	2343*
EI-D-01-15	34	Plant macrofossil	1055 ± 35	924-1000	962
EI-D-01-15	35.86	Plant macrofossil	6355 ± 20	7257-7311	7284*
EI-P-01-15	39.5	Plant macrofossil	3030 ± 20	3179-3275	3227*
EI-D-01-15	40.2	Plant macrofossil	8110 ± 45	8985-9125	9055*
EI-P-01-15	43.86	Plant macrofossil	3915 ± 20	4316-4400	4358*
EI-D-01-15	57	Bulk organic matter	2450 ± 15	2471-2673	2572
EI-P-01-15	60.36	Bulk organic matter	2330 ± 20	2337-2355	2346
EI-D-01-15	82	Bulk organic matter	3300 ± 15	3492-3547	3520*
EI-P-01-15	96.16	Plant macrofossil	2945 ± 15	3076-3142	3109
EI-P-01-15	138.26	Plant macrofossil	3595 ± 15	3865-3925	3895
EI-P-01-15	138.86	Hekla-S Tephra			3750
EI-P-01-15	156.86	Hekla-4 Tephra			4260
EI-P-01-15	164.46	Plant macrofossil	4100 ± 30	4519-4703	4611
EI-P-01-15	174.96	Plant macrofossil	4310 ± 15	4844-4870	4857
EI-P-01-15	263.46	Bulk organic matter	7290 ± 30	8059-8145	8102
EI-P-01-15	278.46	Plant macrofossil	7925 ± 20	8645-8817	8731
EI-P-01-15	301.46	Saksunarvatn tephra			10176

* indicates anomalously old radiocarbon ages that were not included in the final Eiðisvatn age model.

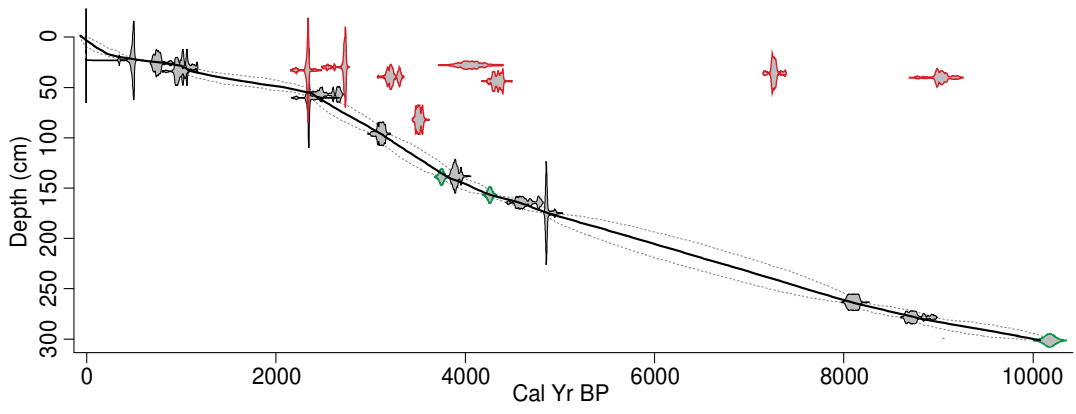

Figure 4. Age model for Eiðisvatn sediment cores constructed using 'Bacon' in R (Blaauw and Christen, 2011). Grey shaded areas are probability distribution functions for individual dates. Red outlined symbols indicate radiocarbon outliers that were removed from the final age model. Black outlined symbols indicate radiocarbon ages that were used in the final age model. Green outlined symbols indicate tephra ages. Solid black line indicates median age model, and dashed line indicates 95% confidence interval. The average 95% confidence interval for sample ages is 454 years and the average amount of time represented by a 1cm-thick sample is 33 years.

4.1.3 EI-P-01-15 301.5 cm/Saksunarvatn Ash (c. 10.2 ka BP)

The major oxide composition of most glass shards from the visible tephra horizon at the 140.5-141.5 cm (n=24) depth interval closely resembles previously described deposits of the c. 10.2 ka BP basaltic Saksunarvatn Ash in the Faroe Islands (Wastegård et al., 2001; Kylander et al., 2012; Lohne et al., 2013; Table 1, Figure 3). The Saksunarvatn Ash, with origins in the Grímsvotn volcanic system, is one of the most widely-dispersed Icelandic tephra deposits from the Holocene.

4.2 Holocene Lithology and Biomarker Relative Abundances

The Eiðisvatn sediment core is comprised primarily of dark brown gyttja. Fine laminations are visible in the bottom ~30 cm of the core, and the core terminates in a visible tephra layer. The sediment has an average LOI of ~15%, but ranges from 0% in the bottom tephra layer to 44%.

376 The Eiðisvatn record was divided into four units based on the lithostratigraphy, biomarker
377 abundances (Figure 5), and isotope stratigraphy (Figure 6).
378
379 Unit 1 (~10.0–8.1 ka) is the basal unit, which is comprised of finely laminated sediment with
380 relatively low LOI (average of ~8.2%). This unit also has high relative abundances of C_{17} and
381 C_{19} *n*-alkanes, which are typically attributed to algal and bacterial sources. The average *n*-alkane
382 ACL is 29.3, and the average *n*-alkanoic acid ACL is 26.5.
383
384 Unit 2 (~8.1– 4.0 ka) is comprised of dark brown gyttja, and has an average LOI of ~14%. The
385 LOI increases steadily throughout Unit 2. The average *n*-alkane ACL is 29.4 and the average *n*-
386 alkanoic acid ACL is 26.5. The sample from the Hekla-4 cryptotephra horizon has a low *n*-
387 alkane ACL of 27.7 and also a low LOI value of 4.8%.
388
389 Unit 3 (4.0 – 2.4 ka) is also a dark brown gyttja, and has an average LOI of 17%. While the LOI
390 increased steadily throughout Units 1 and 2, LOI is more variable in Unit 3, with two small,
391 broad peaks that increase to ~20%. Both *n*-alkane and *n*-alkanoic acid ACLs decline across Unit
392 3, with average values of 29.1 and 26.3, respectively.

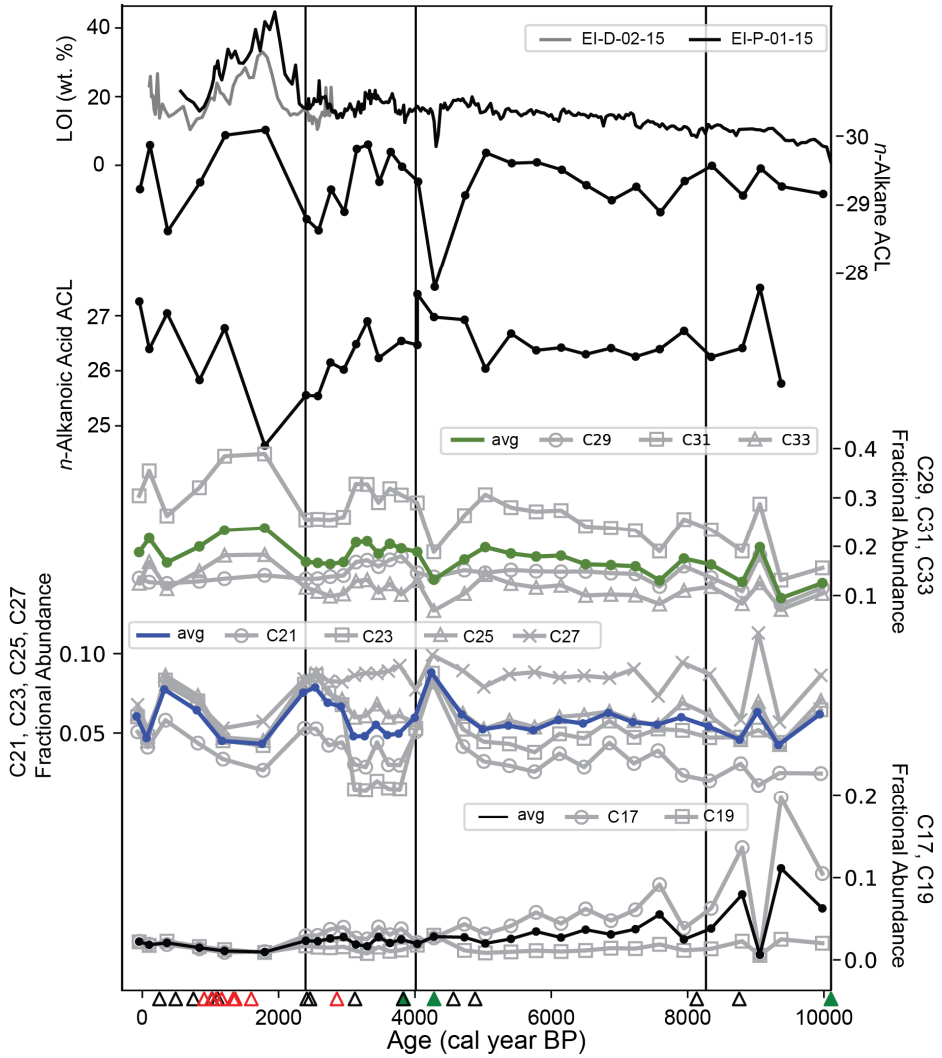

393 Figure 5. Weight % Loss on Ignition measurements and plant wax distributions for the Holocene
394 sediment core from Eiðisvatn. Triangles along x-axis indicate chronological tie points. Red
395 triangles indicate radiocarbon age reversals that were excluded from age model, black triangles
396 indicate radiocarbon ages that were included, and green triangles indicate tephra layers.

397

398 Unit 4 (2.4 – 0 ka) is the uppermost unit. This unit is a darker brown gyttja, and has an average
399 LOI of ~27%. While the LOI increased almost linearly across Units 1-3, this unit has a large
400 peak in LOI up to the maximum of 44%, which corresponds to the darkest interval in the core
401 and also the anomalously old radiocarbon ages that were rejected from the age-depth model.

Because this unit is characterized by an influx of apparently old carbon, it is possible that the radiocarbon ages that were not rejected from the model may also be older than the actual age of the sediment (Figure 4). Thus, the age of the lower boundary of this unit is tentative, and further interpretation regarding the age of this transition should be made with caution. The *n*-alkane ACL increases to ~30 during the LOI peak while the *n*-alkanoic acid ACL decreases to 24.6. Average *n*-alkane ACL across Unit 4 is 29.4, and average *n*-alkanoic acid ACL is 26.2.

4.3 δD and $\delta^{13}C$ of plant waxes

4.3.1 δD of Holocene plant waxes

The plant waxes are grouped into in four different categories (Figure 6): long-chain *n*-alkanes, including C_{29}, C_{31}, and C_{33}; mid-chain *n*-alkanes, including C_{25} and C_{27}; long-chain *n*-alkanoic acids, including C_{28}, C_{30}, and C_{32}; and mid-chain *n*-alkanoic acids, including C_{22}, C_{24}, and C_{26}.

The long-chain *n*-alkanes are most variable in Unit 1, where all homologues show a ~20‰ decrease in δD values between 9.3 ka and 9.0 ka and reach their minimum at 9.0 ka. After the initial drop, C_{31} and C_{33} δD values slowly increase upwards while C_{29} δD values remain stable. In Unit 1, C_{33} has the most positive δD values, followed by C_{31} δD values, and C_{29} δD values are the most negative. In Unit 2 (~8.1 – 4.0 ka), C_{31} δD values and C_{33} δD values increase slightly while C_{29} δD values remain stable. After ~6.0 ka, C_{31} δD values become more positive than C_{29} δD values. δD values of all three homologues are stable throughout Unit 3. In Unit 4, their δD values decrease from 2.4 ka to 0.355 ka, after which they increase to the present.

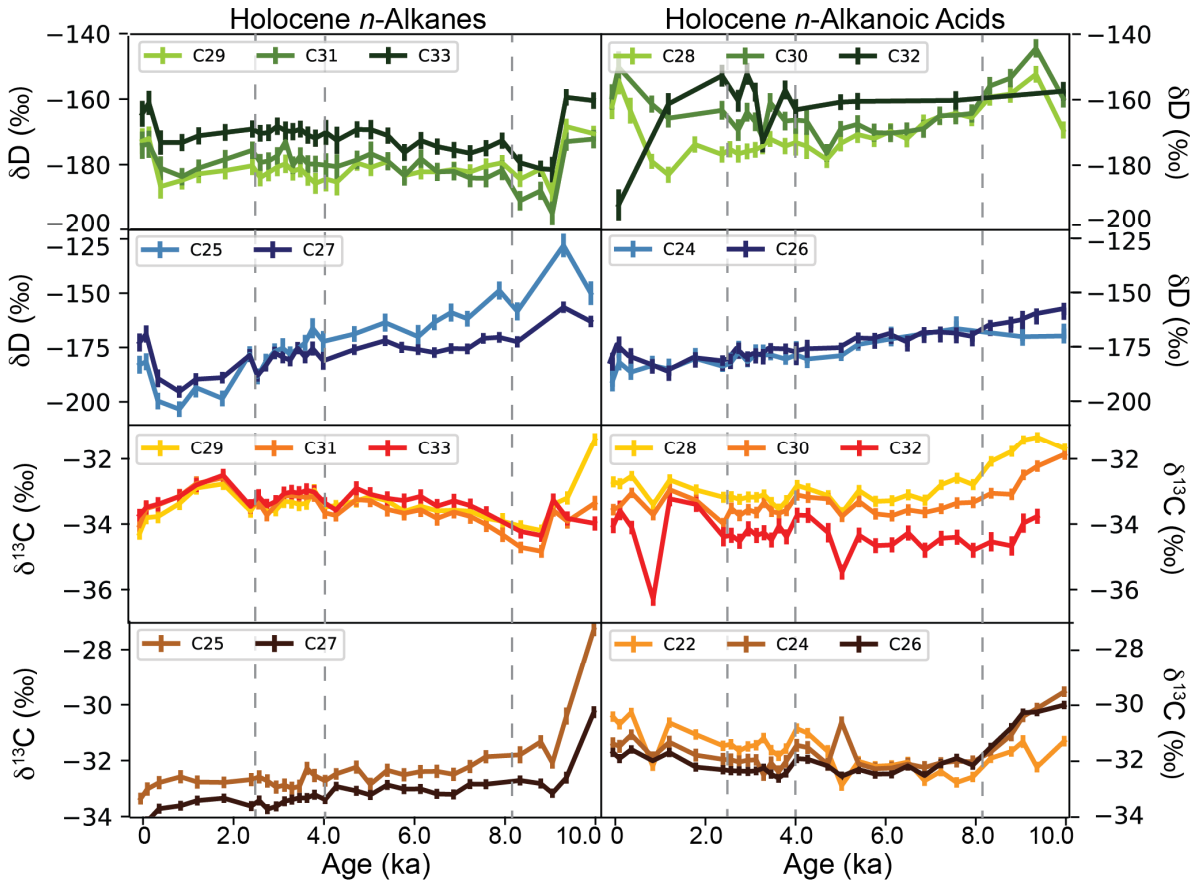

425 Figure 6. Holocene *n*-alkane (left column) and *n*-alkanoic acid (right column) isotope values
426 from the Eiðisvatn record. Green and blue panels show δD data for long- and mid-chain
427 homologues, respectively. Red and brown panels show $\delta^{13}C$ data for long-chain and mid-chain
428 homologues, respectively. Darkest color in each panel indicates longest chain length. Vertical
429 dashed lines indicate Unit boundaries, as in Figures 5 and 7.
430
431
432
433
434

435 Mid-chain *n*-alkane (C_{25} and C_{27}) δD values have a different trend during the Holocene
436 compared to long-chain *n*-alkane δD values. Mid-chain *n*-alkane δD values are relatively high
437 during Unit 1, and decrease gradually during Unit 2. In Unit 3, mid-chain *n*-alkane δD values
438 decrease more rapidly. In Units 1-3, C_{25} δD values are more positive than C_{27} δD values,
439 however in Unit 4 C_{27} becomes more positive. In Unit 4, mid-chain *n*-alkane δD values continue
440 to decrease between 4.0 and 0.8 ka, after which they increase to their modern values. Overall,
441 C_{25} values are highest in the earliest Holocene with a peak value of -128‰, and reach their
442 minimum of -203‰ at ~0.8 ka. C_{27} δD values have a smaller range between -156‰ and -195‰.
443
444 In Units 1 and 2, C_{28} and C_{30} long-chain *n*-alkanoic acid δD values have a trend similar to the
445 mid-chain *n*-alkanes. They have greatest values in Unit 1, and then slowly decrease throughout
446 Unit 2. C_{28} δD values then remain stable throughout Unit 3, but the C_{30} *n*-alkanoic acid becomes
447 more positive by ~10‰. In Unit 4, C_{28} δD values decrease from 2.0 to 1.2 ka, and then increase
448 until present. C_{30} δD values remain stable from 2.0 to 1.2 ka, and then also increase until present.
449 The C_{32} *n*-alkanoic acid was not abundant enough to measure δD on every sample but the δD
450 values were more positive than the other homologues and generally follow the variability of C_{30}
451 δD values in the later part of the record, then falling to the lowest Holocene value in the
452 uppermost sample.
453
454 Mid-chain *n*-alkanoic acid δD values are less variable than any of the other homologues' δD
455 values. In Unit 1, C_{26} δD values slowly decline while C_{24} δD values remain stable. Both C_{24} and

456 C_{26} δD values decrease steadily across Units 2 and 3. In Unit 4, C_{24} continues to decrease, while
457 C_{26} decreases from 2.4 to 1.2 ka, and then increases until present.
458
459 *4.3.2 $\delta^{13}C$ of Holocene plant waxes*
460
461 Long-chain *n*-alkane $\delta^{13}C$ values mirror the long-chain δD values, with a sharp drop in Unit 1,
462 slow rise through Unit 2, and relative stability during Unit 3. At the beginning of Unit 4 there is a
463 1‰ increase followed by decline to present. With the exception of the oldest sample (10.0 ka),
464 C_{29}, C_{31}, and C_{33} $\delta^{13}C$ values are within analytical uncertainty of each other and follow the same
465 trend.
466
467 The trends in the mid-chain *n*-alkane $\delta^{13}C$ values are less variable than mid-chain δD values,
468 with the exception of the $\delta^{13}C$ value of the oldest sample which is ~2.5-3‰ more positive than
469 the next oldest sample. Mid-chain *n*-alkane $\delta^{13}C$ values decline across Units 1 and continue to
470 decline until ~7.0ka in Unit 2. C_{25} $\delta^{13}C$ values are stable through the rest of Units 2-4, until the
471 decline from 355 cal yr BP to the present. C_{25} $\delta^{13}C$ values are more positive than C_{27} $\delta^{13}C$ values
472 in each sample. C_{27} $\delta^{13}C$ values are more positive than long-chain *n*-alkane $\delta^{13}C$ values in Units
473 1 and 2, but are more negative in Units 3 and 4. C_{25} values are more positive than long-chain *n*-
474 alkane $\delta^{13}C$ values in each sample.
475
476 Long-chain *n*-alkanoic acid $\delta^{13}C$ values have differing trends over the Holocene. C_{28} and C_{30}
477 slowly decline in Unit 1 and Unit 2 until ~7.0 ka. They are stable for the remainder of the record,
478 through Units 2-4. The trends in C_{32} $\delta^{13}C$ values, however, are more similar to long-chain *n*-

alkane $\delta^{13}C$ values. They decline abruptly in Unit 1, increase across Unit 2, and are relatively stable during Unit 3. The C_{32} $\delta^{13}C$ values then increase across the transition into Unit 4 and decline until present (with one outlier).

Of the mid-chain *n*-alkanoic acids, C_{26} and C_{24} $\delta^{13}C$ values decline across Unit 1 and remain stable across Units 2 and 3. They increase throughout Unit 4 to present. C_{22} $\delta^{13}C$ values are ~1.5‰ more negative than C_{26} and C_{24} at the beginning of Unit 1 and are relatively stable across this interval. C_{22} $\delta^{13}C$ values are stable across Unit 2 until an abrupt increase ~ 5.0 ka, and then remain stable for the remainder of Unit 3. C_{22} $\delta^{13}C$ values then increase across Unit 4.

4.3.3 δD and $\delta^{13}C$ of LIG plant waxes

LIG long-chain *n*-alkane δD values (Figure 7) show little variability over the length of the record. C_{29} δD values are the most positive, followed by $C_{33,}$ and C_{31} δD values, which are the most negative. Long-chain *n*-alkane δD values have averages of -174‰, -179‰, and -176‰ for C_{29}, C_{31}, and C_{33}, respectively. Mid-chain *n*-alkane δD values also show little variability. C_{25} δD values are slightly more positive in some samples, but C_{27} and C_{25} δD values are within analytical uncertainty of one other for most samples. The average C_{25} δD value for this record is -170‰, and the average C_{27} value is -173‰.

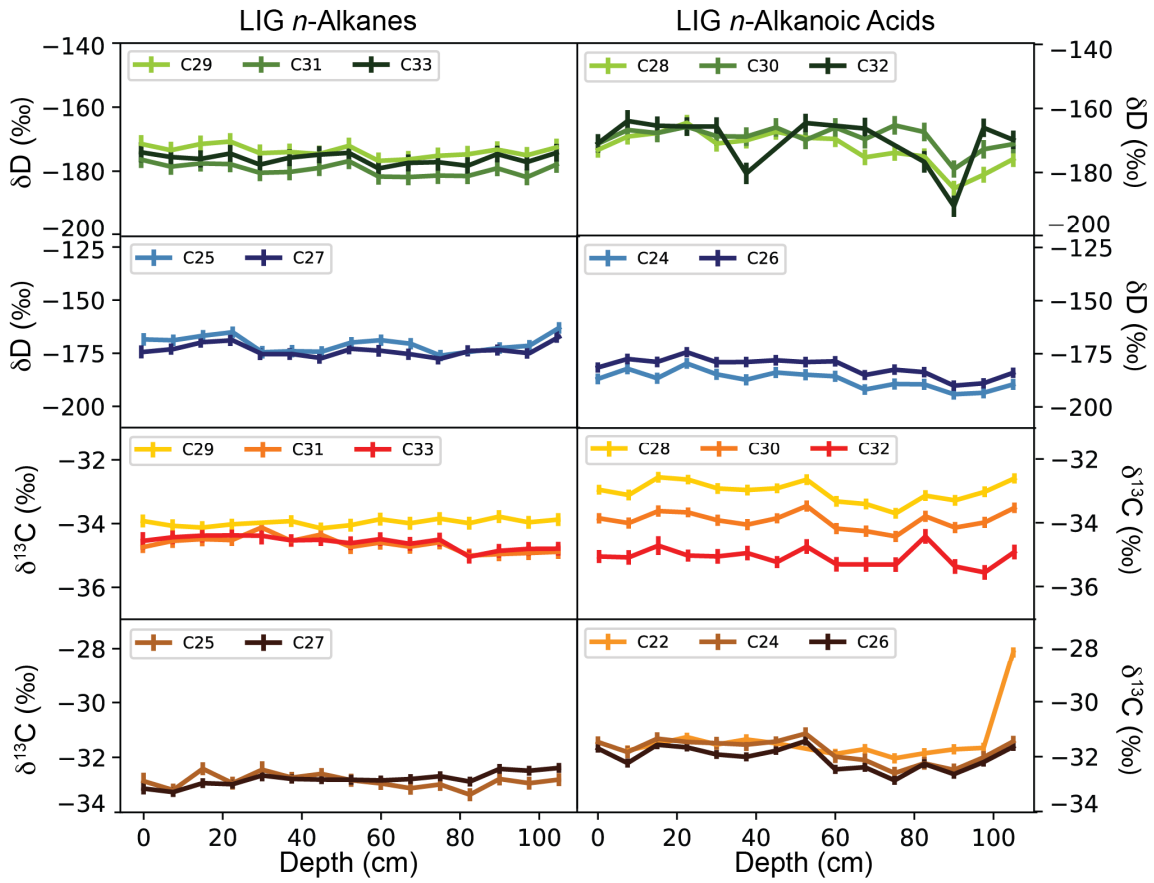

Figure 7. LIG *n*-alkane (left column) and *n*-alkanoic acid (right column) isotope values from the Klaksvík section. Green and blue panels show δD data for long- and mid-chain homologues, respectively. Red and brown panels show $\delta^{13}C$ data for long-chain and mid-chain homologues, respectively. Darkest color in each panel indicates longest chain length.

LIG long-chain *n*-alkanoic acid δD values (Figure 7) also show little variability, with the exception of one sample (depth = 82.5cm) in which all three homologues are more negative. C_{30} δD values are more positive than C_{28} δD values, and they have average values of -169‰ and -172‰ , respectively. The LIG mid-chain *n*-alkanoic acids also have low variability in δD values. The δD values of C_{24} are slightly more positive than those of C_{26}, with an average δD value of -187‰, and C_{26} has an average δD value of -181‰.

LIG wax $\delta^{13}C$ values (both *n*-alkanes and *n*-alkanoic acids) are also relatively constant within the section. C_{33} and C_{31} *n*-alkane $\delta^{13}C$ values are the same (within error), while C_{29} $\delta^{13}C$ values are slightly more positive. C_{33} and C_{31} $\delta^{13}C$ values both average -34.6‰, and C_{29} has an average value of -34.0‰. The mid-chain *n*-alkane $\delta^{13}C$ values are very similar to each other, and are both more positive than the long-chain *n*-alkane $\delta^{13}C$ values. C_{27} has an average value of -32.8‰ and C_{25} has an average value of -32.9‰.

Long-chain *n*-alkanoic acid $\delta^{13}C$ values are consistently offset from one another by ~1‰. The average $\delta^{13}C$ values for C_{28}, C_{30}, and C_{32} are -33.0‰, -33.9‰, and -35.1‰, respectively. The mid-chain *n*-alkanoic acid $\delta^{13}C$ values are very similar to one another, with the exception of one outlier. The mid chai*n-n*-alkanoic acids $\delta^{13}C$ values are also more positive than the long-chain values, with average values of -31.7‰, -31.8‰ , and -32.1‰ for C_{22}, C_{24}, and C_{26}, respectively.

5. Discussion

5.1 Plant wax sources

Understanding the sources of plant waxes is important for interpreting the climate signals contained in the δD records. Plant wax molecules are usually attributed to different types of vegetation according to the length of their carbon chains; short-chain lipids (17-20 carbon atoms) are produced by aquatic algae and bacteria, mid-chain lipids (21-26 carbon atoms) are produced by submerged aquatic plants, and long-chain lipids (27-35 carbon atoms) are produced in the leaf waxes of terrestrial plants (Cranwell et al., 1987; Eglinton and Hamilton, 1967; Ficken et al., 2000). While individual plant species may produce a variety of chain lengths (Diefendorf et al., 2011), when integrated through space and time in a sedimentary record, the isotopes of hydrogen and carbon in the biomarkers can be attributed to more specific sources than isotopes of organic material in bulk sediment (Sachse et al., 2012). If different individual or groups of waxes can be attributed to primarily aquatic or terrestrial sources, then past changes in precipitation isotopes and local hydroclimate can be inferred (Rach et al., 2017; Sachse et al., 2012; Seki et al., 2011).

The trends in the δD values of *n*-alkanes and *n*-alkanoic acids in the Eiðisvatn record can be grouped by wax type and the chain length (Figure 8). We would expect that waxes derived from the same sources have similar trends in δD values, even if the values are offset. Notably, the long-chain and mid-chain *n*-alkane δD values show very different trends, and the δD records of all chain lengths of *n*-alkanoic acids are more similar to the mid-chain *n*-alkane δD records in units 1-3 (Figure 8). From this, we infer that the long-chain *n*-alkanes record a signal from one

555 source (terrestrial plants), while the mid-chain *n*-alkanes and the *n*-alkanoic acids record a signal
556 from another source (aquatic macrophytes).
557
558 While all wax groups likely receive contributions from both terrestrial and aquatic sources, the
559 carbon isotope ratio ($\delta^{13}C$) of plant waxes can provide insight concerning the dominant sources
560 of individual plant wax homologues. The $\delta^{13}C$ of plant waxes reflect the isotopic composition of
561 their CO_2 source, in addition to the fractionation that occurs during biosynthesis. Terrestrial
562 plants source CO_2 from the atmosphere, while aquatic plants source CO_2 from lake water
563 dissolved inorganic carbon (DIC). DIC is generally enriched in ^{13}C due to the uptake of ^{12}C by
564 photosynthetic organisms in surface waters (Meyers and Teranes, 2001). This can cause aquatic
565 plants to be enriched in ^{13}C compared to terrestrial plants, which has been observed in the Faroe
566 Islands and in similar environments in Iceland (Langdon et al., 2010; Olsen et al., 2010). The
567 carbon isotopic enrichment of aquatically sourced waxes is evident within the wax groups, in
568 that shorter carbon chains have more positive $\delta^{13}C$ values than longer chains in almost every
569 sample from both Eiðisvatn (Figure 6) and the Klaksvík section (Figure 7), and previous studies
570 report that there is no systematic difference in $\delta^{13}C$ values of homologous waxes from individual
571 plants (Chikaraishi and Naraoka, 2007, 2003). Therefore, while each homologue within a
572 sediment sample likely represents a mixture of sources, we can use $\delta^{13}C$ values as an indicator of
573 whether aquatic or terrestrial components are the dominant source for each homologue.
574
575 The *n*-alkanoic acids from Eiðisvatn and Klaksvík sediment are more enriched in ^{13}C than would
576 be expected given the $\delta^{13}C$ value of the biosynthetically equivalent *n*-alkane, which suggests that
577 they are predominantly produced by an aquatic macrophyte source. Modern plant studies of $\delta^{13}C$

578 across wax types show that *n*-alkanes are enriched compared to their *n*-alkanoic acid biosynthetic
579 equivalents (Chikaraishi and Naraoka, 2007) by up to 7‰ in $\delta^{13}C$. The apparent fractionation of
580 ^{13}C between *n*-alkanes and *n*-alkanoic acids ($\varepsilon_{13Calk\text{-}13Cacid}$) averages 1.4 ± 1.1‰ regardless of
581 plant type or photosynthetic pathway (Chikaraishi and Naraoka, 2007). We would thus expect
582 the sedimentary waxes to have similar $\varepsilon_{13Calk\text{-}13Cacid}$ values if they are derived from the same
583 source. $\varepsilon_{13Calk\text{-}13Cacid}$ values calculated for the C_{30} *n*-alkanoic acid/C_{29} *n*-alkane, the C_{28} *n*-
584 alkanoic acid/C_{27} *n*-alkane, and the C_{26} *n*-alkanoic acid/C_{25} *n*-alkane from Holocene samples in
585 the Faroe Islands are less than 1.4‰ in most samples, and in many cases $\varepsilon_{13Calk\text{-}13Cacid}$ is negative
586 (Figure 8). This implies that the *n*-alkanoic acid $\delta^{13}C$ values are more positive than they would
587 be if they had the same source as the *n*-alkanes, which supports our interpretation that the *n*-
588 alkanoic acids are primarily aquatically sourced.
589
590 While long-chain *n*-alkanoic acids are commonly attributed to terrestrial sources, in some
591 settings *n*-alkanoic acids as long as C_{28} have been found to be aquatically-derived or from mixed
592 sources (Holland et al., 2013; van Bree et al., 2018). In the Eiðisvatn sediments, $\varepsilon_{13Calk\text{-}13Cacid}$
593 values for the C_{32} *n*-alkanoic acid are the most positive, suggesting that C_{32} *n*-alkanoic acids have
594 more of a terrestrial signature than the other *n*-alkanoic acids. However, in these samples the C_{32}
595 *n*-alkanoic acid has very low abundances, making it difficult to measure its δD values. The trend
596 in the δD values of the C_{30} *n*-alkanoic acid are consistent with the mid-chain *n*-alkane δD records
597 only from 10.0 ka to ~6.0 ka, and during this period $\varepsilon_{13Calk\text{-}13Cacid}$ is very low, which is consistent
598 with a predominantly aquatic source. In the latter half of the Holocene, the δD values of the C_{30}
599 *n*-alkanoic acid no longer follow the trend of the mid-chain *n*-alkane δD record, however they do

not exactly follow the long-chain *n*-alkane δD trend either. The C_{30} *n*-alkanoic acid is likely derived from a mixture of terrestrial and aquatic sources, reflected in the higher $\varepsilon_{13Calk\text{-}13Cacid}$ values from ~6.0ka to present.

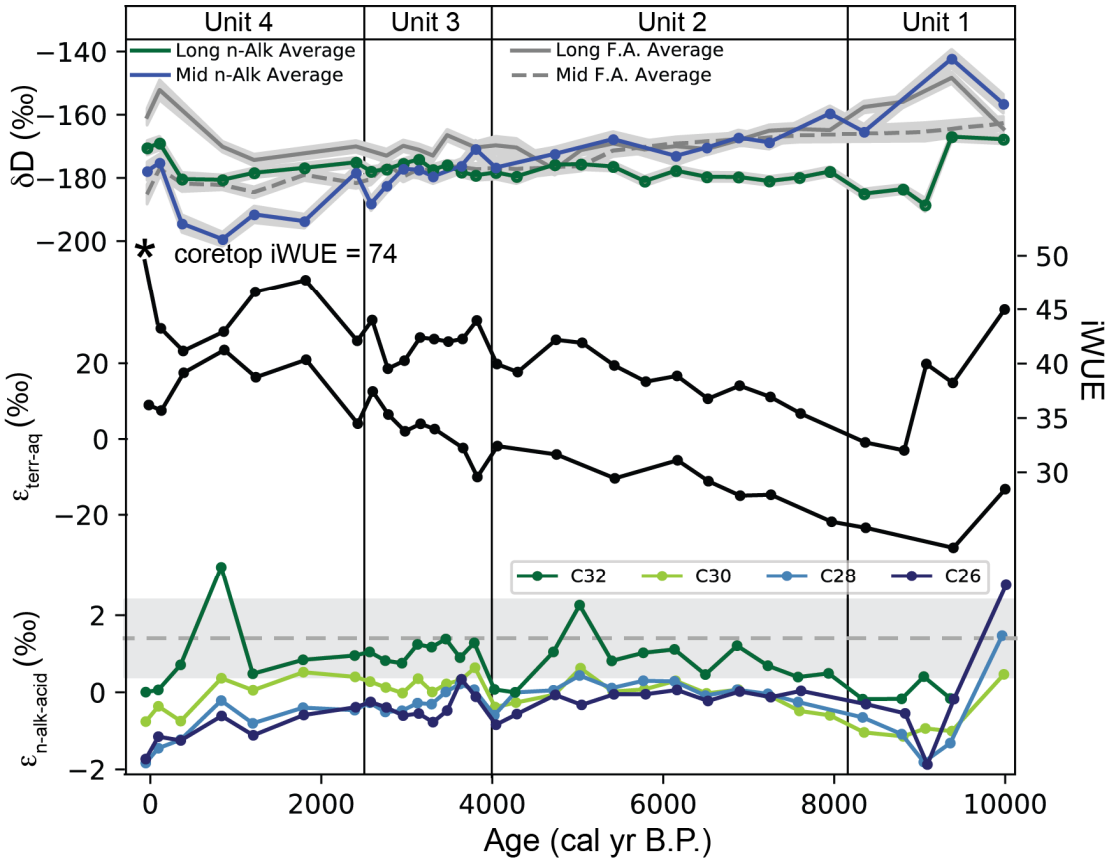

Figure 8. Top: Average *n*-alkane and *n*-alkanoic acid δD values in the Holocene (green: long-chain *n*-alkane δD values, blue: mid-chain *n*-alkane δD values, solid grey: long-chain *n*-alkanoic acid δD values, dashed grey: mid-chain *n*-alkanoic acid δD values). Middle: Hydroclimate proxies in the Holocene record, including calculated iWUE and $\varepsilon_{terr\text{-}aq}$. Bottom: Calculated offset between biosynthetically equivalent *n*-alkanes and *n*-alkanoic acids ($\varepsilon_{n\text{-}alk\text{-}acid}$) for each sample in the Holocene record. Grey dashed line and shaded region indicates published average value ± 1σ error.

Trends in the Holocene $\varepsilon_{13Calk\text{-}13Cacid}$ values reveal changes in the relative proportion of terrestrial and aquatic contributions to the plant waxes that are preserved. The $\varepsilon_{13Calk\text{-}13Cacid}$ values for all the plant wax pairs are most negative during Unit 1, indicating that the proportion of aquatically derived *n*-alkanoic acids was greatest at this time, or that the *n*-alkanoic acids that are produced have more positive $\delta^{13}C$ values. This suggests that there was a higher proportion of autochthonous material being deposited in Eiðisvatn in the early Holocene, which can either be accomplished by a reduction in terrestrial input or enhanced aquatic productivity. Unit 1 also has the highest relative abundances of C_{17} and C_{19} *n*-alkanes, the production of which is attributed to algae (Cranwell et al., 1987), which is also consistent with a higher proportion of autochthonous organic matter being deposited. Pollen records suggest that following deglaciation around 11.2 ka, the early Holocene in the Faroes was characterized by fell-field vegetation and poor soil development (Hannon et al., 2010, 2003; Johansen, 1985). If the terrestrial biomass was small and soils were thin, there would be less terrestrially sourced material delivered to the lake. $\varepsilon_{13Calk\text{-}13Cacid}$ values for all wax pairs are stable throughout Units 2 and 3, and decline again in Unit 4. This suggests that the proportion of aquatic vs terrestrial *n*-alkanoic acids is relatively constant through the mid-Holocene, and the latest Holocene is characterized by a slightly increased aquatic contribution.

5.2 Holocene climate

5.2.1 Precipitation isotopes

In the Faroe Islands, the δD of lake water represents the isotopic composition of precipitation, and therefore we interpret mid-chain *n*-alkane and *n*-alkanoic acid δD values as recorders of past

precipitation isotopes. In a wet, cool environment, like the Faroes, evaporative enrichment of lake water is minimal. Lake water collected from Faroese lakes that are currently hydrologically open have δD and $\delta^{18}O$ compositions that fall on the local meteoric water line for the Reykjavik GNIP station (Figure 2), indicating that little evaporation has occurred. The average δD values of these lake water samples (-36.5‰) are very similar to the OIPC modeled precipitation for August (-39‰), the month that the samples were collected. Because the mid-chain *n*-alkanes and most of the *n*-alkanoic acids (C_{30} and shorter) are primarily aquatically derived, we expect that they are recording past changes in lake water isotopes during the growing season, from which we can infer past changes in spring-summer precipitation isotopes.

Precipitation δD values at mid-latitudes are strongly influenced by regional temperatures, changes in moisture source and/or local changes in hydroclimate. The location, temperature, and relative humidity of the oceanic moisture source influence the initial isotopes of precipitation in a given air mass; the trajectory of the air mass, amount of rainfall along that trajectory, and additional moisture added to the air mass through evaporation of surface waters influence the intermediate isotopic composition; the seasonality of precipitation and the local temperature and relative humidity during condensation affect the final isotopes of precipitation (Boyle, 1997; Dansgaard, 1964; Pierrehumbert, 1999). In the North Atlantic today, heat and moisture carried northward by ocean and atmospheric transport cause the region (including the Faroe Islands) to have anomalously positive isotopes in precipitation for its latitude (Bowen and Revenaugh, 2003).

Given the numerous controls on precipitation isotopes in the region, rather than interpreting precipitation isotopes strictly as a quantitative indicator of temperature, we use the δD data to infer regional climatology. During periods with enhanced northward oceanic heat transport by the North Atlantic Current, for instance due to more vigorous meridional overturning circulation, greater heat and moisture are transported to the North Atlantic resulting in more positive precipitation isotopes values in the North Atlantic region. During periods with reduced northward oceanic heat transport, for instance due to weaker overturning circulation, regional temperatures cool, less Atlantic-sourced precipitation reaches the Faroe Islands and the moisture that does is subject to greater rainout and isotopic fractionation prior to arrival, and the isotopes in precipitation become more negative.

In our Eiðisvatn record, δD values of mid-chain *n*-alkanes and *n*-alkanoic acids indicate an overall decrease in the isotope values of precipitation during the course of the Holocene (Figure 8). We interpret this trend to reflect a decrease in the northward transport of heat and moisture in the North Atlantic region. This trend generally matches the declining trend in Northern Hemisphere summer insolation and the documented decline in regional summer temperatures over the same period (Marcott et al., 2013). The most positive isotope values in the Eiðisvatn record occur during Unit 1, suggesting an early regional thermal maximum. A major decline begins within Unit 3, likely signaling cooling temperatures and less Atlantic-sourced precipitation during the Neoglacial period. These trends broadly match local qualitative temperature records from the Faroe Islands, which indicate a thermal maximum ~9.0 to 8.0 ka, cooling from ~8.0 ka to 4.0 ka, and intensified cooling until present (Hannon et al., 2010; Johansen, 1985, 1981; Olsen et al., 2010). This is also consistent with the closest Holocene sea

surface temperature reconstruction, which shows peak Holocene temperatures from 10.3 ka to 8.3 ka and declining temperatures until modern (Rasmussen and Thomsen, 2010). Regional SSTs also generally match this trend (Ayache et al., 2018; Marcott et al., 2013; Marsicek et al., 2018). The reason for increased northward ocean heat transport in the early to mid-Holocene is likely linked to enhanced overturning circulation and deep water convection processes in the Nordic seas at this time (Thornalley et al., 2013).

We note that the decrease in precipitation δD values throughout the Holocene in the Faroe Islands could also be interpreted as a shift toward a greater amount of wintertime precipitation. However, we reject this interpretation on a number of grounds. Firstly, δD values of plant waxes are likely to be biased toward precipitation isotope values during the growing season, i.e. spring and summer. The isotopic values of modern lake water samples are most similar to precipitation in the month that they were collected (August) rather than the mean annual precipitation value predicted by OIPC. This suggests that the δD values of aquatically derived plant waxes are likely recording lake water/precipitation water δD values in late spring and summer and would not reflect seasonal changes in precipitation isotopes. Secondly, the seasonal range in the isotopes of precipitation of the Faroe Islands, as calculated by the OIPC (Bowen, 2019), is relatively small (~50‰; Figure 2). Even under the most extreme case, assuming 100% of annual precipitation in the Early Holocene fell during the summer season, precipitation isotope values would not increase by the magnitude inferred from the plant wax δD values; instead, the data indicate that early Holocene precipitation isotopes were more positive than in the late Holocene. Additionally, because OIPC-predicted summer precipitation isotope values may be overestimated, it is even

701 less likely that seasonal shifts alone can account for the inferred 35‰ decrease in precipitation
702 isotope values over the Holocene.
703
704 *5.3 Holocene hydroclimate*
705
706 The difference between a terrestrial plant-derived wax δD record (δD_{terr}) and an aquatic-plant-
707 derived wax δD record (δD_{aq}) represents watershed-integrated soil water evaporative enrichment
708 and plant evapotranspiration, which are generally attributed to changes in relative humidity
709 (Nichols et al., 2010; Rach et al., 2017; Seki et al., 2011). As stated in Section 5.2, Faroese lake
710 water isotopes are expected to reflect changes in precipitation isotopes because the lake water
711 experiences little evaporative enrichment, and thus mid-chain plant wax δD values track
712 precipitation isotopes. But, soil and therefore leaf waters can experience evaporative enrichment,
713 depending on local relative humidity (Sachse et al., 2004; Ziegler, 1989). A comparison of plant
714 water and lake water isotope reconstructions based on long-chain and mid-chain wax δD values,
715 respectively, can reflect evaporative enrichment of precipitation water, which can be attributed to
716 changes in local hydroclimate (Nichols et al., 2010; Rach et al., 2017; Seki et al., 2011). We
717 interpret the fractionation between δD_{terr} and δD_{aq} ($\varepsilon_{2Hterr\text{-}2Haq}$) to represent the amount of
718 evaporative enrichment of soil and leaf water. We find an increasing trend in $\varepsilon_{2Haq\text{-}2Hterr}$ after 9.0
719 ka, indicating a drying trend over most of the Holocene (Figure 8).
720
721 Carbon isotope values of terrestrial plant waxes can also reflect local hydrology. In terrestrial
722 plants, the fractionation of carbon isotopes during photosynthesis is controlled by the
723 fractionation associated with gas diffusion through the stomata and the fractionation of the

724 Rubisco enzyme (Farquhar et al., 1982). When the environment becomes drier, the stomata on a
725 plant's leaves close to reduce evaporative loss of water, which reduces the fractionation between
726 atmospheric CO_2 and plant wax carbon, increasing plant wax $\delta^{13}C$ values. Therefore, terrestrial
727 plant carbon isotopes can also be used to infer past changes in moisture due to changes in leaf-
728 level isotopic fractionation ($\varepsilon_{13Catm\text{-}13Cplant}$) that are associated with changing stomatal
729 conductance and intrinsic water use efficiency (iWUE) (Ehleringer et al., 1993). iWUE increases
730 over the Holocene, which is consistent with the drying trend interpreted from $\varepsilon_{2Haq\text{-}2Hterr}$.
731
732 Changes in carbon assimilation that are unrelated to moisture availability can also impact the
733 water use efficiency of plants and can complicate $\delta^{13}C$-based hydroclimate interpretations. If
734 other environmental factors such as increased light exposure or increased nutrients increase the
735 photosynthetic capacity of a plant, c_i is reduced and the carbon isotopic values of plant material
736 become enriched, which is also expected at higher iWUE. Mesophyll conductance, or the
737 diffusion of CO_2 between substomatal cavities to the cite of CO_2 fixation, is also an important
738 factor for iWUE that is independent of hydrologically-driven changes in stomatal conductance
739 (Seibt et al., 2008). By evaluating δD and $\delta^{13}C$ together, those effects can be disentangled; if δD
740 and $\delta^{13}C$ co-vary it is likely that changes in relative humidity are the drivers (Scheidegger et al.,
741 2000), while a negative correlation suggests a change in photosynthetic capacity as the main
742 driver of $\delta^{13}C$ changes. iWUE shows similar trends to $\varepsilon_{2Haq\text{-}2Hterr}$ (Figure 8), with higher iWUE
743 when there is more inferred evaporative enrichment of water isotopes. Thus, we infer from both
744 proxies that a reduction in relative humidity occurred throughout the course of the Holocene.
745

746 Shifts in vegetation type in the watershed can also affect plant wax δD and $\delta^{13}C$ values,
747 independent of hydroclimatic change. The shift in long-chain plant wax δD and $\delta^{13}C$ around 9.3
748 ka is likely due to a change in vegetation. The period between 10.5 ka and 9.0 ka was
749 characterized by a rapid rise and decline of *Betula nana* and a rapidly changing climate in the
750 Faroe Islands (Hannon et al., 2010, 2003; Jessen et al., 2008; Johansen, 1985, 1981, 1975), after
751 which the climate became more mild and vegetation became dominated by sedges, heath, and
752 juniper scrub. After 9.0 ka and before 2.4 ka, there is no indication of major, sudden shifts in
753 vegetation based on plant wax distributions (Figure 5) or from published pollen records that span
754 the Holocene (Johansen, 1985, 1975).
755
756 Hydroclimate reconstructions from the Arctic and North Atlantic regions are scarce compared to
757 temperature reconstructions (Sundqvist et al., 2014), however they are critical to understanding
758 past changes in the climate system. Reconstructions of glacier size in western Norway, which are
759 thought to be dominantly controlled by winter precipitation amount, suggest that some regions
760 experienced wetter conditions in the neoglacial period (Bakke et al., 2008) while others
761 experienced drier conditions (Bjune et al., 2005). Pollen and lake level records from Northern
762 Scandinavia also diverge, with some indicating a drying trend over the Holocene (Bigler et al.,
763 2002; Hammarlund et al., 2003) and some showing little hydrological changes after 6.0 ka
764 (Seppa and Birks, 2001). Southern Scandinavian lake levels appear to have increased after 4.0 ka
765 (Hammarlund et al., 2003), and a reduction in the humification of peat in northern Scotland after
766 3.9 ka indicate wetter neoglacial conditions (Anderson et al., 1998). Our results from the Faroe
767 Islands suggest a shift to drier conditions in the late Holocene.
768

769 *5.4 The last 2.4 ka*

770

771 The Eiðisvatn core provides evidence for a major environmental shift beginning at ~2.4 ka (Unit
772 4). This is perhaps most obvious in the LOI signal, which increases to ~40 % during this time. At
773 the same time as the LOI peak, there are eight anomalously old radiocarbon ages. This implies a
774 sudden input of old organic material, indicating rapid erosion that is documented elsewhere in
775 the Faroes during the late Holocene (Hannon et al., 2005; Lawson et al., 2005; Olsen et al.,
776 2010). Associated with the peak in LOI, there is an increase in the $\delta^{13}C$ values of long-chain *n*-
777 alkanes (Figure 6), potentially due to changes in vegetation associated with peat and/or grassland
778 formation in the watershed. Additionally, there is a notable change in the distribution of plant
779 waxes after 2.4 ka, primarily a large increase in the amount of C_{31} and C_{33} *n*-alkanes leading to
780 higher *n*-alkane ACL (Figure 5). C_{31} and C_{33} are often attributed to grasses (Maffei, 1996), and
781 this probably reflects a transition to grassland from a heath, sedge, and shrub-dominated
782 landscape.

783

784 The environmental shift that is recorded at 2.4 ka in the Eiðisvatn record could be explained by
785 early human settlement on the Faroe Islands. Evidence from pollen records confirm that large,
786 wild grass types (which, on Iceland, are an indication of human settlement) were present before
787 2.82 ka (Hannon and Bradshaw, 2000). The first microcharcoal evidence of human settlement
788 was dated to 1.38 ka (Hannon et al., 2005). A paleobotanical settlement horizon at Eiðisvatn was
789 dated to between 1.3-1.55 ka (Hannon et al., 2001). Our evidence of landscape change predates
790 the pollen evidence significantly; however, uncertainties in the age model after 2.4 ka make it
791 difficult to conclude whether this disturbance interval is linked to the paleobotanical changes

observed by Hannon et al., 2001 and others, or if it indicates that erosion began to occur before the appearance of cereals and charcoal. Because of a lack of tall, deep-rooting plants, it is possible that the landscape was particularly sensitive to minor changes in climate, and late-Holocene cooling triggered erosion in the watershed. Without compelling evidence of human settlement in the Faroes during this disturbance interval, it cannot be attributed to either human or climate drivers.

5.5 Interglacial climate comparison

Mid-chain alkane δD values from the late LIG Klaksvík sediment, which are interpreted to represent precipitation δD, are similar to Holocene δD values from 8.1-4.0 ka (Figure 9), and are approximately 20‰ more positive than the average for the last 2.4 ka. This implies that late LIG regional temperatures were higher than the late Holocene, but similar to those of the early and middle Holocene. Furthermore, the late LIG $\varepsilon_{2Hterr\text{-}2Haq}$ values are most similar to Holocene values from Unit 2, and late LIG iWUE values are most similar to Holocene values from Unit 1

807 (Figure 9), suggesting that the late LIG was wetter than the mid-late Holocene. Previous studies
808 of the Klaksvík LIG section have found *Ajuga,* statoblasts of *Cristatella mucedo*, and *Betula*
809 sect. *Albae*, which suggest that summer temperatures were slightly higher than modern
810 conditions (Bennike et al., 2018; Wastegård et al., 2005). Other than those few differences, most
811 of the pollen and macrofossils from the late LIG section in the Faroes indicate that the vegetation

812 was similar to the pre-settlement vegetation of the Holocene (Bennike et al., 2018; Wastegård et
813 al., 2005).

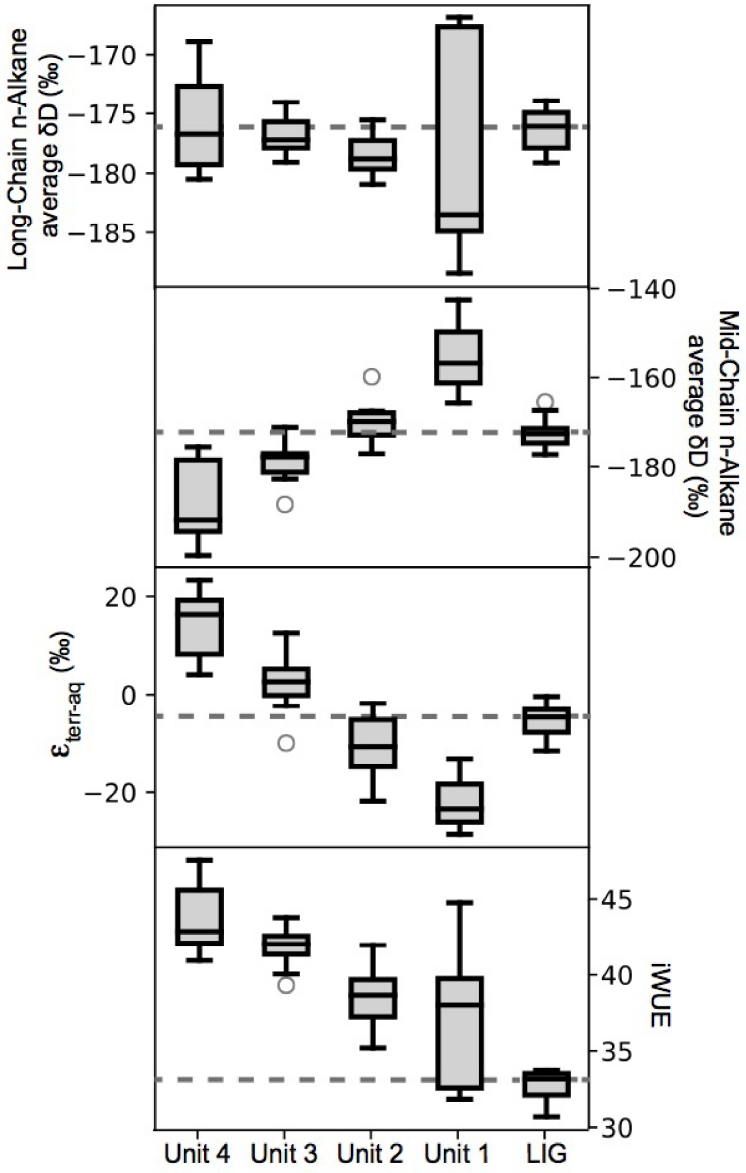

814 Figure 9. Comparison of LIG and Holocene plant wax δD values and paleohydrological proxies
815 in the Faroe Islands. Box and whisker plots for each unit of the Holocene record for comparison
816 to all LIG values. Dashed grey line indicates mean of the LIG values.

817 Global temperatures during the LIG are generally thought to have been higher than the present
818 interglacial due to higher summer insolation, evidenced by higher temperatures in the Greenland
819 (NEEM Community Members, 2013) and Antarctic (Jouzel et al., 2007) ice core records, sea
820 level that was 6-9m higher than present (Dutton et al., 2015), various marine and terrestrial proxy
821 records (Capron et al., 2014; Kaspar et al., 2005; Turney and Jones, 2010), and climate model
822 simulations (Gierz et al., 2017; Otto-Bliesner et al., 2013). As discussed in section 5.2.1, the δD
823 of precipitation in this location represents temperature, moisture sources, and regional
824 temperature gradients related to the amount of ocean and atmospheric heat transport from lower
825 latitudes. Modeling studies of precipitation isotopes during the LIG indicate that annually
826 averaged precipitation isotopes may have been more negative in the North Atlantic during the
827 LIG compared to modern (Gierz et al., 2017). Summer precipitation shows slightly more positive
828 isotope values in the North Atlantic for the 125 ka time slice, but more negative values for 120
829 and 130 ka (Gierz et al., 2017). This suggests that even if global temperatures were warmer and
830 precipitation isotopes in other regions were more positive, the North Atlantic and more
831 specifically the Faroe Islands may be an exception, and overall the climate in this part of the
832 North Atlantic may have been very similar to the Holocene during the LIG.
833
834 Because of the uncertainty inherent in dating terrestrial LIG archives, it is difficult to ascertain
835 precisely which part of the LIG the Klaksvík section captures, however previous studies have
836 suggested that it encompasses the late LIG and does not include the beginning of the LIG period.
837 Greve (2001) inferred that the Klaksvík sequence spans approximately 5ky-8ky after 124 ka
838 through a comparison of the Klaksvík pollen sequence to European pollen sequences from the
839 Eemian (Zagwijn, 1996) and the presence of the 53-Midt/RHY tephra. Given the Holocene

840 sedimentation rate we observe in our Eiðisvatn record, it is reasonable that the ~1m of LIG
841 sediment could represent 5-8 ky of the late LIG. The chronological uncertainties for the LIG
842 section at Klaksvík are not unique to this location, due to the difficulties in dating terrestrial
843 material from the LIG. However, the section at Klaksvík still provides a useful snapshot of late
844 LIG conditions at this North Atlantic site.
845
846 Paleoclimate records and modeling studies show different peak warming periods during the LIG
847 (Capron et al., 2014; Otto-Bliesner et al., 2013; Pfeiffer and Lohmann, 2016). Some marine
848 records in the North Atlantic and the NEEM ice core show early peak warming (~130ka),
849 followed by cooling, generally matching the LIG northern hemisphere summer insolation curve
850 (Cortijo et al., 1994; Fronval et al., 1998; Manthé, 1998; Oppo et al., 2006). However, the two
851 closest marine sea surface temperature records (MD95-2009 and ENAM 33) on either side of the
852 Iceland-Faroe Ridge show late peak warmth, after the deposition of the 53-Midt/RHY tephra that
853 is present in both the Klaksvík section and the MD95-2009 record (Capron et al., 2014; Manthé,
854 1998; Rasmussen et al., 2003). While it is possible that peak warmth occurred early in the LIG,
855 and that the late LIG sequence preserved in the Faroe Islands does not encompass the warmest
856 interval of the LIG period, these local sea surface temperature records suggest delayed warming
857 in the North Atlantic region relative to insolation forcing, unlike Holocene SST records and our
858 record from the Faroes, which suggests that regional temperatures and northward moisture
859 transport were closely tied to insolation forcing and peaked during the early Holocene. Van
860 Nieuwenhove et al., 2011 attribute the delayed incursion of warm North Atlantic waters in the
861 Nordic Seas to lingering effects of the Saalian Ice Sheet and the boundary conditions created by
862 different ice sheet configurations following Termination II. Although our data cannot speak to

863 conditions during the early LIG, they do indicate warmer-than-present conditions during the late
864 LIG period and are consistent with local SST records that suggest late LIG warming.
865
866 Despite the age uncertainties of the Klaksvík sediment, comparison of the same climate proxy in
867 nearly the same geographic locations allows us to place this snapshot of the late LIG in the
868 context of the climate evolution of the Holocene. It is well-established that most of the North
869 Atlantic and Arctic was warmest during the early- to mid-Holocene, and that preindustrial and
870 Little Ice Age temperatures are potentially the coldest since the last glacial period or the Younger
871 Dryas (Marcott et al., 2013; Marsicek et al., 2018). Here, we infer that late LIG conditions in this
872 region were similar to early Holocene conditions.
873

874 **6. Conclusion**

875 We report Holocene and late Last Interglacial (LIG) paleoclimate reconstructions from Lake
876 Eiðisvatn on the island of Eysturoy and a lacustrine sediment unit from Klaksvík, Borðoy Island
877 in the Faroe Islands, based on hydrogen and carbon isotopes of sedimentary plant waxes. The
878 trends in hydrogen isotope values of terrestrially- and aquatically-derived plant waxes are used to
879 infer that the Faroe Islands became progressively drier and that there was a reduction in the
880 northward transport of heat by the ocean and atmosphere to the northern North Atlantic
881 throughout the course of the Holocene. This conclusion is based on the interpretation that the
882 hydrogen isotopes of long-chain *n*-alkanes reflect the isotopic composition of soil and leaf water
883 that was subject to isotopic enrichment due to evaporation, while the shorter chain *n*-alkanes
884 reflect lake water that tracks precipitation isotopes. The carbon isotopes of long-chain *n*-alkanes,
885 which reflect the intrinsic water use efficiency of terrestrial plants, support this interpretation and

886 suggest that moisture availability decreased throughout the Holocene. This study provides the
887 first Holocene paleohydrologic reconstruction for the Faroe Islands. By comparing the same
888 climate proxy measurements to those made on plant waxes preserved in late LIG-aged
889 sediments, we are able to place the climate conditions of the late LIG in the Faroe Islands into
890 the context of Holocene climate and to conclude that late LIG climate in the Faroe Islands was
891 warmer and wetter than present, and most similar to the conditions of the mid to early Holocene.

892

893 **Acknowledgements**

894 This research was supported by NSF grant NSF-BCS-16-23595 to WJD, NB, and RB. We would
895 like to thank Jostein Bakke for assistance in the field, and Nicole DeRoberts for assistance in the
896 LDEO Organic Geochemistry Laboratory. We also acknowledge two anonymous reviewers,
897 whose comments helped to improve this manuscript.

898 **References**
899
900 Anderson, D.E., Binney, H.A., Smith, M.A., 1998. Evidence for abrupt climatic change in
901 northern Scotland between 3900 and 3500 calendar years BP. The Holocene 8, 97–103.
902 Andresen, C.S., Björck, S., Rundgren, M., Conley, D.J., Jessen, C., 2006. Rapid Holocene
903 climate changes in the North Atlantic: evidence from lake sediments from the Faroe Islands.
904 Boreas 35, 23–34. https://doi.org/10.1080/03009480500359228
905 Arge, S. V., Sveinbjarnardóttir, G., Edwards, K.J., Buckland, P.C., 2005. Viking and medieval
906 settlement in the Faroes: People, place and environment. Hum. Ecol. 33, 597–620.
907 https://doi.org/10.1007/s10745-005-4745-1
908 Axford, Y., Briner, J.P., Cooke, C.A., Francis, D.R., Michelutti, N., Miller, G.H., Smol, J.P.,
909 Thomas, E.K., Wilson, C.R., Wolfe, A.P., 2009. Recent changes in a remote Arctic lake are
910 unique within the past 200,000 years 0–3.
911 Ayache, M., Swingedouw, D., Mary, Y., Eynaud, F., Colin, C., 2018. Multi-centennial
912 variability of the AMOC over the Holocene : A new reconstruction based on multiple
913 proxy-derived SST records. Glob. Planet. Change 170, 172–189.
914 https://doi.org/10.1016/j.gloplacha.2018.08.016
915 Bakke, J., Lie, Ø., Dahl, S.O., Nesje, A., Bjune, A.E., 2008. Strength and spatial patterns of the
916 Holocene wintertime westerlies in the NE Atlantic region. Glob. Planet. Change 60, 28–41.
917 https://doi.org/10.1016/j.gloplacha.2006.07.030
918 Baldini, L.M., McDermott, F., Foley, A.M., Baldini, J.U.L., 2008. Spatial variability in the
919 European winter precipitation δ18O-NAO relationship: Implications for reconstructing
920 NAO-mode climate variability in the Holocene. Geophys. Res. Lett. 35, L04709.
921 https://doi.org/10.1029/2007GL032027
922 Bauch, H.A., Erlenkeuser, H., Fahl, K., Spielhagen, R.F., Weinelt, M.S., Andruleit, H., 1999.
923 Evidence for a steeper Eemian than Holocene sea surface temperature gradient between
924 Arctic and sub-Arctic regions. Palaeogeogr. Palaeoclimatol. Palaeoecol. 145, 95–117.
925 Behl, R.J., Kennett, J.P., 1996. Brief interstadial events in the Santa Barbara basin, NE Pacific,
926 during the past 60 kyr. Nature. https://doi.org/10.1038/379243a0
927 Bennike, O., Hedenäs, L., Lemdahl, G., Wiberg-Larsen, P., 2018. A multiproxy macrofossil
928 record of Eemian palaeoenvironments from Klaksvík, the Faroe Islands. Boreas 47, 106–
929 113. https://doi.org/10.1111/bor.12254
930 Bigler, C., Larocque, I., Peglar, S.M., Hall, R.I., 2002. Quantitative multiproxy assessment of
931 long-term patterns of Holocene environmental change from a small lake. The Holocene 12,
932 481–496.
933 Björck, S., Noe-Nygaard, N., Wolin, J., Houmark-Nielsen, M., Jørgen Hansen, H., Snowball, I.,
934 2000. Eemian Lake development, hydrology and climate: A multi-stratigraphic study of the
935 Hollerup site in Denmark. Quat. Sci. Rev. 19, 509–536. https://doi.org/10.1016/S0277-
936 3791(99)00025-6
937 Bjune, A.E., Bakke, J., Nesje, A., Birks, H.J.B., 2005. Holocene mean July temperature and
938 winter precipitation in western Norvay inferred from palynological and glaciological lake-
939 sediment proxies. The Holocene 15, 177–189.
940 Blaauw, M., Christen, J.A., 2011. Flexible paleoclimate age-depth models using an
941 autoregressive gamma process. Bayesian Anal. 6, 457–474. https://doi.org/10.1214/11-
942 BA618
943 Blockley, S.P.E., Pyne-O'Donnell, S.D.F., Lowe, J.J., Matthews, I.P., Stone, A., Pollard, A.M.,

Turney, C.S.M., Molyneux, E.G., 2005. A new and less destructive laboratory procedure for the physical separation of distal glass tephra shards from sediments. Quat. Sci. Rev. 24, 1952–1960. https://doi.org/10.1016/J.QUASCIREV.2004.12.008
Bowen, G.J., 2019. The Online Isotopes in Precipitation Calculator, version 3.1.
Bowen, G.J., Revenaugh, J., 2003. Interpolating the isotopic composition of modern meteoric precipitation. Water Resour. Res. 39, 1–13. https://doi.org/10.1029/2003WR002086
Bowen, G.J., Wassenaar, L.I., Hobson, K.A., 2005. Global application of stable hydrogen and oxygen isotopes to wildlife forensics. Oecologia 143, 337–348. https://doi.org/10.1007/s00442-004-1813-y
Boyle, E.A., 1997. Cool tropical temperatures shift the global d18O-T relationship: An explanation for the ice core d18O-borehole thermometry conflict? Geophys. Res. Lett. 24, 273–276.
Broecker, W.S., Bond, G., Klas, M., Bonani, G., Wolfi, W., 1990. A Salt Oscillator in the Glacial Atlantic? 1. The Concept. Paleoceanography 5, 469–477.
CAPE-Last Interglacial Project Members, 2006. Last Interglacial Arctic warmth confirms polar amplification of climate change. Quat. Sci. Rev. 25, 1383–1400. https://doi.org/10.1016/j.quascirev.2006.01.033
Cappelen, J., 2018. Weather observations from Tórshavn, The Faroe Islands 1953-2017.
Capron, E., Govin, A., Stone, E.J., Mulitza, S., Otto-bliesner, B., Rasmussen, T.L., Sime, L.C., Waelbroeck, C., Wolff, E.W., 2014. Temporal and spatial structure of multi-millennial temperature changes at high latitudes during the Last Interglacial. Quat. Sci. Rev. 103, 116–133. https://doi.org/10.1016/j.quascirev.2014.08.018
Chikaraishi, Y., Naraoka, H., 2007. d13C and dD relationships among three n-alkyl compound classes (n-alkanoic acid, n-alkane and n-alkanol) of terrestrial higher plants. Org. Geochem. 38, 198–215. https://doi.org/10.1016/j.orggeochem.2006.10.003
Chikaraishi, Y., Naraoka, H., 2003. Compound-specific δD-δ13C analyses of n-alkanes extracted from terrestrial and aquatic plants. Phytochemistry 63, 361–371. https://doi.org/10.1016/S0031-9422(02)00749-5
Chikaraishi, Y., Naraoka, H., 2001. Organic hydrogen-carbon isotope signatures of terrestrial higher plants during biosynthesis for distinctive photosynthetic pathways. Geochem. J. 35, 451–458. https://doi.org/10.2343/geochemj.35.451
Chikaraishi, Y., Naraoka, H., Poulson, S.R., 2004. Carbon and hydrogen isotopic fractionation during lipid biosynthesis in a higher plant (Cryptomeria japonica). Phytochemistry 65, 323–330. https://doi.org/10.1016/j.phytochem.2003.12.003
Clark, P.U., Pisias, N.G., Stocker, T.F., Weaver, A.J., 2002. The role of thermohaline circulation in abrupt climate change. Nature 415, 863–869. https://doi.org/10.1038/415863a
CLIMAP Project Members, 1984. The Last Interglacial Ocean. Quat. Res. 21, 123–224. https://doi.org/10.1016/0033-5894(84)90098-X
Collister, J.W., Rieley, G., Stern, B., Eglinton, G., Fry, B., 1994. Compound-specific d13C analyses of leaf lipids from plants with differing carbon dioxide metabolisms. Org. Geochem. 21, 619–627. https://doi.org/10.1016/S1352-0237(01)00321-5
Cortijo, E., Duplessy, J.C., Labeyrie, L., Leclaire, H., Dupart, J., van Weering, T.C.E., 1994. Eemian cooling in the Norwegian Sea and North Atlantic ocean preceding continental ice-sheet growth. Nat. Clim. Chang. 372, 446–449.
Cranwell, P.A., Eglinton, G., Robinson, N., 1987. Lipids of aquatic organisms as potential contributors to lacustrine sediments--ll *. Org. Geochem. 11, 513–527.

Dansgaard, W., 1964. Stable isotopes in precipitation. Tellus 16, 436–468. https://doi.org/10.3402/tellusa.v16i4.8993
De Beaulieu, J.-L., Reille, M., 1992. The Last Climatic Cycle at La Grande Pile (Vosges, France): A New Pollen Profile. Quat. Sci. Rev. 11, 431–438.
Diefendorf, A.F., Freeman, K.H., Wing, S.L., Graham, H. V., 2011. Production of n-alkyl lipids in living plants and implications for the geologic past. Geochim. Cosmochim. Acta 75, 7472–7485. https://doi.org/10.1016/j.gca.2011.09.028
Dutton, A., Carlson, A.E., Long, A.J., Milne, G.A., Clark, P.U., DeConto, R., Horton, B.P., Rahmstorf, S., Raymo, M.E., 2015. Sea-level rise due to polar ice-sheet mass loss during past warm periods. Science 349, aaaa4019. https://doi.org/10.1126/science.aaa4019
Eglinton, G., Hamilton, R.J., 1967. Leaf Epicuticular Waxes. Science 156, 1322–1335.
Ehleringer, J.R., Hall, A.E., Farquhar, G.D. (Eds.), 1993. Stable Isotopes and Plant Carbon-Water Relations. Academic Press, San Diego.
Elsig, J., Schmitt, J., Leuenberger, D., Schneider, R., Eyer, M., Leuenberger, M., Joos, F., Fischer, H., Stocker, T.F., 2009. Stable isotope constraints on Holocene carbon cycle changes from an Antarctic ice core. Nature 461, 507–510. https://doi.org/10.1038/nature08393
Farquhar, G.D., O'Leary, M.H., Berry, J.A., 1982. On the Relationship between Carbon Isotope Discrimination and the Intercellular Carbon Dioxide Concentration in Leaves. Aust. J. Plant Physiol. 9, 121–137.
Feakins, S.J., 2013. Pollen-corrected leaf wax D/H reconstructions of northeast African hydrological changes during the late Miocene. Palaeogeogr. Palaeoclimatol. Palaeoecol. 374, 62–71. https://doi.org/10.1016/j.palaeo.2013.01.004
Feng, X., 1999. Trends in intrinsic water-use efficiency of natural trees for the past 100–200 years: A response to atmospheric CO2 concentration. Geochim. Cosmochim. Acta 63, 1891–1903.
Ficken, K.J., Li, B., Swain, D.L., Eglinton, G., 2000. An n-alkane proxy for the sedimentary input of submerged/floating freshwater aquatic macrophytes. Org. Geochem. 31.
Fronval, T., Jansen, E., Haflidason, H., Sejrup, H.P., 1998. Variability in Surface and Deep Water conditions in the Nordic Seas Durin ghte Last Interglacial Period. Quat. Sci. Rev. 17.
Geikie, J., 1881. On the Geology of the Færöe Islands. Trans. R. Soc. Edinburgh 30, 217–269. https://doi.org/10.1017/S0080456800029033
Gierz, P., Werner, M., Lohmann, G., 2017. Simulating climate and stable water isotopes during the Last Interglacial using a coupled climate-isotope model. J. Adv. Model. Earth Syst. 9, 2027–2045. https://doi.org/10.1002/2017MS001056
Hammarlund, D., Björk, S., Buchardt, B., Israelson, C., Thomsen, C.T., 2003. Rapid hydrological changes during the Holocene revealed by stable isotope records of lacustrine carbonates from Lake Igelsjön, southern Sweden. Quat. Sci. Rev. 22, 353–370.
Hannon, G.E., Bradshaw, R.H.W., 2000. Impacts and timing of the first human settlement on vegetation of the Faroe Islands. Quat. Res. 54, 404–413. https://doi.org/10.1006/qres.2000.2171
Hannon, G.E., Bradshaw, R.H.W., Bradshaw, E.G., Snowball, I., Wastegård, S., 2005. Climate change and human settlement as drivers of late-Holocene vegetational change in the Faroe Islands. The Holocene 5, 639–647.
Hannon, G.E., Bradshaw, R.H.W., Wastegård, S., 2003. Rapid vegetation change during the early Holocene in the Faroe Islands detected in terrestrial and aquatic ecosystems. J. Quat.

Sci. 18, 615–619. https://doi.org/10.1002/jqs.783
Hannon, G.E., Hermanns-Auðardóttir, M., Wastegård, S., 1998. Human Impact at Tjørnuvík in the Faroe Islands. FróDskaparrit 46, 215–228.
Hannon, G.E., Rundgren, M., Jessen, C.A., 2010. Dynamic early Holocene vegetation development on the Faroe Islands inferred from high-resolution plant macrofossil and pollen data. Quat. Res. 73, 163–172. https://doi.org/10.1016/j.yqres.2009.11.003
Hannon, G.E., Wastegård, S., Bradshaw, E., Bradshaw, R.H.W., 2001. Human impact and landscape degradation on the Faroe Islands. Biol. Environ. Proc. R. Irish Acad. 101B, 129–139.
Heiri, O., Lotter, A.F., Lemcke, G., 2001. Loss on ignition as a method for estimating organic and carbonate content in sediments: reproducibility and comparability of results. J. Paleolimnol. 25, 101–110.
Holland, A.R., Petsch, S.T., Castaneda, I.S., Wilkie, K.M., Burns, S.J., Brigham-Grette, J., 2013. A biomarker record of Lake El'gygytgyn , Far East Russian Arctic: investigating sources of organic matter and carbon cycling during marine isotope stages 1-3. Clim. Past 9, 243–260. https://doi.org/10.5194/cp-9-243-2013
Holland, M.M., Bitz, C.M., 2003. Polar amplification of climate change in coupled models. Clim. Dyn. 21, 221–232. https://doi.org/10.1007/s00382-003-0332-6
Hou, J., Andrea, W.J.D., Huang, Y., 2008. Can sedimentary leaf waxes record D/H ratios of continental precipitation? Field, model, and experimental assessments. Geochim. Cosmochim. Acta 72, 3503–3517. https://doi.org/10.1016/j.gca.2008.04.030
Jessen, C.A., Rundgren, M., Björck, S., Andresen, C.S., Conley, D.J., 2008. Variability and seasonality of North Atlantic climate during the early Holocene: evidence from Faroe Island lake sediments. The Holocene 18, 851–860.
Johansen, J., 1985. Studies in the vegetational history of the Faroe and Shetland Islands. Ann. Soc. Sci. Færoensis Suppl. 11.
Johansen, J., 1981. Vegetational development in the Faroes from 10,000 BP to the present. Årbog-Dansmarks Geol. undersøgelse 111–136.
Johansen, J., 1975. Pollen Diagrams from the Shetland and Faroe Islands. New Phytol. 75, 369–387.
Jørgensen, G., Rasmussen, J., 1986. Glacial striae, roches moutonnées, and ice movements in the Faroe Islands.
Jouzel, J., Mason-Delmotte, V., Cattani, O., Dreyfus, G., Falourd, S., Hoffmann, G., Minster, B., Nouet, J., Barnola, J.M., Chappellaz, J., Fischer, H., Gallet, J.C., Johnsen, S., Leuenberger, M., Loulergue, L., Luethi, D., Oerter, H., Parrenin, F., Raisbeck, G., Raynaud, D., Schilt, A., Schwander, J., Selmo, E., Souchez, R., Spahni, R., Stauffer, B., Steffensen, J.P., Stenni, B., Stocker, T.F., Tison, J.L., Werner, M., Wolff, E.W., 2007. Orbital and Millennial Antarctic Climate Variability over the Past 800,000 Years. Science 317, 793–796.
Kahmen, A., Schefuß, E., Sachse, D., 2013. Leaf water deuterium enrichment shapes leaf wax n-alkane δD values of angiosperm plants II: Observational evidence and global implications. Geochim. Cosmochim. Acta 111, 39–49. https://doi.org/10.1016/j.gca.2012.09.003
Kaspar, F., Ku, N., Cubasch, U., Litt, T., 2005. A model-data comparison of European temperatures in the Eemian interglacial. Geophys. Res. Lett. 32, 1–5. https://doi.org/10.1029/2005GL022456
Kühl, N., Litt, T., 2003. Quantitative time series reconstruction of Eemian temperature at three European sites using pollen data. Veg. Hist. Archaeobot. 12, 205–214.

https://doi.org/10.1007/s00334-003-0019-2
Kukla, G.J., Bender, M.L.B., de Beaulieu, J.-L., Bond, G., Broecker, W.S., Cleveringa, P., Gavin, J.E., Herbert, T.D., Imbrie, J., Jouzel, J., Keigwin, L.D., Knudsen, K.-L., McManus, J.F., Merkt, J., Muhs, D.R., Muller, H., Poore, R.Z., Porter, S.C., Seret, G., Shackleton, N.J., Turner, C., Tzedakis, P.C., Winograd, I.J., 2002. Last Interglacial Climates. Quat. Res. 58, 2–13. https://doi.org/10.1006/qres.2001.2316
Kylander, M.E., Lind, E.M., Wastegård, S., Löwemark, L., 2012. Recommendations for using XRF core scanning as a tool in tephrochronology. Holocene. https://doi.org/10.1177/0959683611423688
Langdon, P.G., Leng, M.J., Holmes, N., Caseldine, C.J., 2010. Lacustrine evidence of early-Holocene environmental change in northern Iceland: A multiproxy palaeoecology and stable isotope study. The Holocene 20, 205–214. https://doi.org/10.1177/0959683609354301
Lawson, I.T., Church, M.J., Edwards, K.J., Cook, G.T., Dugmore, A.J., 2007. Peat initiation in the Faroe Islands: climate change, pedogenesis or human impact? Earth Environ. Sci. Trans. R. Soc. Edinburgh 98, 15–28. https://doi.org/10.1017/S1755691007000035
Lawson, I.T., Church, M.J., McGovern, T.H., Arge, S. V., Woollet, J., Edwards, K.J., Gathorne-Hardy, F.J., Dugmore, A.J., Cook, G., Mairs, K.A., Thomson, A.M., Sveinbjarnardóttir, G., 2005. Historical ecology on Sandoy, Faroe Islands: Palaeoenvironmental and archaeological perspectives. Hum. Ecol. 33, 651–684. https://doi.org/10.1007/s10745-005-7681-1
Lawson, I.T., Edwards, K.J., Church, M.J., Newton, A.J., Cook, G.T., Gathorne-hardy, F.J., Dugmore, A.J., 2008. Human impact on an island ecosystem: pollen data from Sandoy, Faroe Islands. J. Biogeogr. 35, 1130–1152. https://doi.org/10.1111/j.1365-2699.2007.01838.x
LeGrande, A.N., Schmidt, G.A., 2008. Ensemble, water isotope-enabled, coupled general circulation modeling insights into the 8.2 ka event. Paleoceanography 23, PA3207. https://doi.org/10.1029/2008PA001610
Lohne, Ø.S., Mangerud, J., Birks, H.H., 2013. Precise 14C ages of the Vedde and Saksunarvatn ashes and the Younger Dryas boundaries from western Norway and their comparison with the Greenland Ice Core (GICC05) chronology. J. Quat. Sci. 28, 490–500. https://doi.org/10.1002/jqs.2640
Lourantou, A., Chappellaz, J., Barnola, J.-M., Masson-Delmotte, V., Raynaud, D., 2010. Changes in atmospheric CO2 and its carbon isotopic ratio during the penultimate deglaciation. Quat. Sci. Rev. 29, 1983–1992. https://doi.org/10.1016/j.quascirev.2010.05.002
Maffei, M., 1996. Chemotaxonomic significance of leaf wax alkanes in the gramineae. Biochem. Syst. Ecol. 24, 53–64. https://doi.org/10.1016/0305-1978(95)00102-6
Manabe, S., Stouffer, R.J., 1980. Sensitivity of a Global Climate Model to an Increase of CO2 Concentration in the Atmosphere. J. Geophys. Res. 85, 5529–5554.
Mangerud, J., Sønstegaard, E., Sejrup, H.-P., Haldorsen, S., 1981. A continuous Eemian-Early Weichselian sequence containing pollen and marine fossils at Fjøsanger, western Norway. Boreas 10, 137–208.
Manthé, S., 1998. Variabilité de la circulation thermohaline glaciaire et interglaciaire en Atlantique Nord tracée par les foraminifères planctoniques et la microfaune benthique. Université de Bordeaux, France.
Marcott, S.A., Shakun, J.D., Clark, P.U., Mix, A.C., 2013. A Reconstruction of Regional and

Global Temperature for the Past 11,300 Years. Science 339, 1198–1202.
Marsicek, J., Shuman, B.N., Bartlein, P.J., Shafer, S.L., Brewer, S., 2018. Reconciling divergent trends and millennial variations in Holocene temperatures. Nature 554, 92–96. https://doi.org/10.1038/nature25464
McFarlin, J.M., Axford, Y., Osburn, M.R., Kelly, M.A., Osterberg, E.C., Farnsworth, L.B., 2018. Pronounced summer warming in northwest Greenland during the Holocene and Last Interglacial. Proc. Natl. Acad. Sci. 1–6. https://doi.org/10.1073/pnas.1720420115
McKay, N.P., Overpeck, J.T., Otto-Bliesner, B.L., 2011. The role of ocean thermal expansion in Last Interglacial sea level rise. Geophys. Res. Lett. 38, L14605. https://doi.org/10.1029/2011GL048280
Meyers, P.A., Teranes, J.L., 2001. Sediment Organic Matter, in: Last, W.M., Smol, J.P. (Eds.), Tracking Environmental Change Volume 2: Physical and Geochemical Methods. Kluwer Academic Publishers, Dordrecht, The Netherlands, pp. 239–269.
Monnin, E., Steig, E.J., Siegenthaler, U., Kawamura, K., Schwander, J., Stauffer, B., Stocker, T.F., Morse, D.L., Barnola, J.-M., Bellier, B., Raynaud, D., Fischer, H., 2004. Evidence for substantial accumulation rate variability in Antarctica during the Holocene, through synchronization of CO2in the Taylor Dome, Dome C and DML ice cores. Earth Planet. Sci. Lett. 224, 45–54. https://doi.org/10.1016/j.epsl.2004.05.007
NEEM Community Members, 2013. Eemian interglacial reconstructed from a Greenland folded ice core. Nature 493, 489–494. https://doi.org/10.1038/nature11789
Nichols, J., Booth, R.K., Jackson, S.T., Pendall, E.G., Huang, Y., 2010. Differential hydrogen isotopic ratios of Sphagnum and vascular plant biomarkers in ombrotrophic peatlands as a quantitative proxy for precipitation—evaporation balance. Geochim. Cosmochim. Acta 74, 1407–1416. https://doi.org/10.1016/j.gca.2009.11.012
Olsen, J., Björck, S., Leng, M.J., Gudmundsdóttir, E.R., Odgaard, B. V, Lutz, C.M., Kendrick, C.P., Andersen, T.J., Seidenkrantz, M.-S., 2010. Lacustrine evidence of Holocene environmental change from three Faroese lakes : a multiproxy XRF and stable isotope study. Quat. Sci. Rev. 29, 2764–2780. https://doi.org/10.1016/j.quascirev.2010.06.029
Oppo, D.W., McManus, J.F., Cullen, J.L., 2006. Evolution and demise of the Last Interglacial warmth in the subpolar North Atlantic. Quat. Sci. Rev. 25, 3268–3277. https://doi.org/10.1016/j.quascirev.2006.07.006
Otto-Bliesner, B.L., Rosenbloom, N., Stone, E.J., Mckay, N.P., Lunt, D.J., Brady, E.C., Overpeck, J.T., 2013. How warm was the last interglacial? New model–data comparisons. Philos. Trans. R. Soc. 371, 20130097.
Peterson, L.C., Haug, G.H., Hughen, K.A., Röhl, U., 2000. Tropical Atlantic During the Last Glacial Rapid Changes in the Hydrologic Cycle of the Tropical Atlantic During the Last Glacial. Science 290, 1947–1951. https://doi.org/10.1126/science.290.5498.1947
Pfeiffer, M., Lohmann, G., 2016. Greenland Ice Sheet influence on Last Interglacial climate: Global sensitivity studies performed with an atmosphere-ocean general circulation model. Clim. Past 12, 1313–1338. https://doi.org/10.5194/cp-12-1313-2016
Pierrehumbert, R.T., 1999. Huascaran d18O as an indicator of tropical climate during the Last Glacial Maximum. Geophys. Res. Lett. 26, 1345–1348.
Polissar, P.J., D'Andrea, W.J., 2014. Uncertainty in paleohydrologic reconstructions from molecular dD values. Geochim. Cosmochim. Acta 129, 146–156. https://doi.org/10.1016/j.gca.2013.12.021
Polissar, P.J., Freeman, K.H., 2010. Effects of aridity and vegetation on plant-wax δD in modern

lake sediments. Geochim. Cosmochim. Acta 74, 5785–5797. https://doi.org/10.1016/j.gca.2010.06.018
Poynter, J., Eglinton, G., 1990. Molecular Composition of Three Sediments from Hole 717C: The Bengal Fan, Proceedings of the Ocean Drilling Program, Scientific Results, Vol. 116. https://doi.org/10.2973/odp.proc.sr.116.151.1990
Rach, O., Kahmen, A., Brauer, A., Sachse, D., 2017. A dual-biomarker approach for quantification of changes in relative humidity from sedimentary lipid D/H ratios. Clim. Past 13, 741–757.
Rasmussen, J., 1972. Morena a Bordoyarvık, som bendir aeitt millumbil ı glersetingini har norduri. Frodskaparrit 20, 54–70.
Rasmussen, J., Noe-Nygaard, A., 1970. Geology of the Faeroe Islands (Pre-Quaternary). Copenhagen.
Rasmussen, T.L., Thomsen, E., 2010. Holocene temperature and salinity variability of the Atlantic Water inflow to the Nordic seas. Holocene 20, 1223–1234. https://doi.org/10.1177/0959683610371996
Rasmussen, T.L., Thomsen, E., Kuijpers, A., Wastegård, S., 2003. Late warming and early cooling of the sea surface in the Nordic seas during MIS 5e (Eemian Interglacial). Quat. Sci. Rev. 22, 809–821. https://doi.org/10.1016/S0277-3791(02)00254-8
Reimer, P.J., Bard, E., Bayliss, A., Beck, J.W., Blackwell, P.G., Ramsey, C.B., Buck, C.E., Cheng, H., Edwards, R.L., Friedrich, M., Grootes, P.M., Guilderson, T.P., Haflidason, H., Hajdas, I., Hatté, C., Heaton, T.J., Hoffmann, D.L., Hogg, A.G., Hughen, K.A., Kaiser, K.F., Kromer, B., Manning, S.W., Niu, M., Reimer, R.W., Richards, D.A., Scott, E.M., Southon, J.R., Staff, R.A., Turney, C.S.M., van der Plicht, J., 2013. IntCal13 and Marine13 Radiocarbon Age Calibration Curves 0–50,000 Years cal BP. Radiocarbon 55, 1869–1887. https://doi.org/10.2458/azu_js_rc.55.16947
Sachse, D., Billault, I., Bowen, G.J., Chikaraishi, Y., Dawson, T.E., Feakins, S.J., Freeman, K.H., Magill, C.R., McInerney, F.A., van der Meer, M.T.J., Polissar, P., Robins, R.J., Sachs, J.P., Schmidt, H.-L., Sessions, A.L., White, J.W.C., West, J.B., Kahmen, A., 2012. Molecular Paleohydrology: Interpreting the Hydrogen-Isotopic Composition of Lipid Biomarkers from Photosynthesizing Organisms. Annu. Rev. Earth Planet. Sci. 40, 221–249. https://doi.org/10.1146/annurev-earth-042711-105535
Sachse, D., Radke, J., Gleixner, G., 2004. Hydrogen isotope ratios of recent lacustrine sedimentary n-alkanes record modern climate variability. Geochim. Cosmochim. Acta 68, 4877–4889. https://doi.org/10.1016/j.gca.2004.06.004
Salonen, J.S., Helmens, K.F., Brendryen, J., Kuosmanen, N., Väliranta, M., Goring, S., Korpela, M., Kylander, M., Philip, A., Plikk, A., Renssen, H., Luoto, M., 2018. Abrupt high-latitude climate events and decoupled seasonal trends during the Eemian. Nat. Commun. 9, 2851. https://doi.org/10.1038/s41467-018-05314-1
Sauer, P.E., Eglinton, T.I., Hayes, J.M., Schimmelmann, A., Sessions, A.L., 2001. Compound-specific D/H ratios of lipid biomarkers from sediments as a proxy for environmental and climatic conditions. Geochim. Cosmochim. Acta 65, 213–222.
Scheidegger, Y., Saurer, M., Bahn, M., Siegwolf, R., 2000. Linking stable oxygen and carbon isotopes with stomatal conductance and photosynthetic capacity: a conceptual model. Oecologia 125, 350–357. https://doi.org/10.1007/s004420000466
Seibt, U., Rajabi, A., Griffiths, H., Berry, J.A., 2008. Carbon isotopes and water use efficiency: sense and sensitivity. Oecologia 155, 441–454. https://doi.org/10.1007/s00442-007-0932-7

Seki, O., Meyers, P.A., Yamamoto, S., Kawamura, K., Nakatsuka, T., Zhou, W., Zheng, Y., 2011. Plant-wax hydrogen isotopic evidence for postglacial variations in delivery of precipitation in the monsoon domain of China. Geology 39, 875–878. https://doi.org/10.1130/G32117.1

Seppa, H., Birks, H.J.B., 2001. July mean temperature and annual precipitation trends during the Holocene in the Fennoscandian tree-line area: pollen-based climate reconstructions. The Holocene 11, 527–539.

Serreze, M.C., Francis, J.A., 2006. The arctic amplification debate. Clim. Chang. 76, 241–264. https://doi.org/10.1007/s10584-005-9017-y

Shackleton, N.J., Sánchez-Goñi, M.F., Pailler, D., Lancelot, Y., 2003. Marine isotope substage 5e and the Eemian interglacial. Glob. Planet. Change 36, 151–155. https://doi.org/10.1016/S0921-8181(02)00181-9

Sundqvist, H.S., Kaufman, D.S., McKay, N.P., Balascio, N.L., Briner, J.P., Cwynar, L.C., Sejrup, H.P., Seppä, H., Subetto, D.A., Andrews, J.T., Axford, Y., Bakke, J., Birks, H.J.B., Brooks, S.J., de Vernal, A., Jennings, A.E., Ljungqvist, F.C., Rühland, K.M., Saenger, C., Smol, J.P., Viau, A.E., 2014. Arctic Holocene proxy climate database--New approaches to assessing geochronological accuracy and encoding climate variables. Clim. Past 10, 1605–1631. https://doi.org/10.5194/cp-10-1605-2014

Thornalley, D.J.R., Blaschek, M., Davies, F.J., Praetorius, S., Oppo, D.W., McManus, J.F., Hall, I.R., Kleiven, H., Renssen, H., McCave, I.N., 2013. Long-term variations in Iceland-Scotland overflow strength during the Holocene. Clim. Past 9, 2073–2084. https://doi.org/10.5194/cp-9-2073-2013

Turney, C.S.M., Harkness, D.D., Lowe, J.J., 1997. The use of microtephra horizons to correlate Late-glacial lake sediment successions in Scotland. J. Quat. Sci. 12, 525–533.

Turney, C.S.M., Jones, R.T., 2010. Does the Agulhas Current amplify global temperatures during super-interglacials? J. Quat. Sci. 25, 839–843. https://doi.org/10.1002/jqs.1423

van Bree, L.G.J., Peterse, F., van der Meer, M.T.J., Middelburg, J.J., Negash, A.M.D., De Crop, W., Cocquyt, C., Wieringa, J.J., Verschuren, D., Sinninghe Damsté, J.S., 2018. Seasonal variability in the abundance and stable carbon-isotopic composition of lipid biomarkers in suspended particulate matter from a stratified equatorial lake (Lake Chala, Kenya/Tanzania): Implications for the sedimentary record. Quat. Sci. Rev. 192, 208–224. https://doi.org/10.1016/j.quascirev.2018.05.023

Van Nieuwenhove, N., Bauch, H.A., Eynaud, F., Kandiano, E., Cortijo, E., Turon, J., 2011. Evidence for delayed poleward expansion of North Atlantic surface waters during the last interglacial (MIS 5e). Quat. Sci. Rev. 30, 934–946. https://doi.org/10.1016/j.quascirev.2011.01.013

Wang, Y.J., Cheng, H., Edwards, R.L., An, Z.S., Wu, J.Y., Shen, C.-C., Dorale, J.A., 2001. A High-Resolution Absolute-Dated Late Pleistocene Monsoon Record from Hulu Cave , China. Science 294, 2345–2348. https://doi.org/10.1126/science.1064618

Wastegård, S., Björck, S., Grauert, M., Hannon, G.E., 2001. The Mjáuvøtn tephra and other Holocene tephra horizons from the Faroe Islands: a link between the Icelandic source region, the Nordic Seas, and the European continent. The Holocene 11, 101–109. https://doi.org/10.1191/095968301668079904

Wastegård, S., Björck, S., Greve, C., Rasmussen, T.L., 2005. A tephra-based correlation between the Faroe Islands and the Norwegian Sea raises questions about chronological relationships during the last interglacial. Terra Nov. 17, 7–12. https://doi.org/10.1111/j.1365-

3121.2004.00578.x
Wastegård, S., Gudmundsdottir, E.R., Lind, E.M., Timms, R.G.O., Bjorck, S., Hannon, G.E., Olsen, J., Rundgren, M., 2018. Towards a Holocene tephrochronology for the Faroe Islands, North Atlantic. Quat. Sci. Rev. 195, 195–214. https://doi.org/10.1016/j.quascirev.2018.07.024
Wastegård, S., Rundgren, M., Schoning, K., Andersson, S., Björck, S., Borgmark, A., Possnert, G., 2008. Age, geochemistry and distribution of the mid-Holocene Hekla-S/Kebister tephra. Holocene 18, 539–549. https://doi.org/10.1177/0959683608089208
Zagwijn, W.H., 1996. An analysis of Eemian climate in western and central Europe. Quat. Sci. Rev. 15, 451–469. https://doi.org/10.1016/0277-3791(96)00011-X
Zhang, Z., Sachs, J.P., 2007. Hydrogen isotope fractionation in freshwater algae: I. Variations among lipids and species. Org. Geochem. 38, 582–608. https://doi.org/10.1016/j.orggeochem.2006.12.004
Ziegler, H., 1989. Hydrogen Isotope Fractionation in Plant Tissues, in: Rundel, P.W., Ehleringer, J.R., Nagy, K.A. (Eds.), Stable Isotopes in Ecological Research. Springer-Verlag, New York, pp. 105–123.